1 **Expanding seawater carbon dioxide and methane measuring capabilities with a Seaglider**

2

3 Claudine Hauri[1*], Brita Irving[1], Dan Hayes[2], Ehsan Abdi[3,4], Jöran Kemme[5], Nadja Kinski[5], and

4 Andrew M. P. McDonnell[6,7]

5

6 [1]International Arctic Research Center, University of Alaska Fairbanks, Fairbanks, AK 99775,

7 USA

8 [2]Advanced Offshore Operations, Inc., Houston, TX 77004, USA

9 [3]Cyprus Subsea Consulting and Services, Lakatamia 2326, Cyprus

10 [4]now at Akvaplan-Niva, 9296 Tromsø, Norway

11 [5] -4H-JENA engineering GmbH, 07745 Jena, Germany

12 [6] College of Fisheries and Ocean Science, University of Alaska Fairbanks, Fairbanks, AK 99775,

13 USA

14 [7]now at Alaska Renewables, Fairbanks, AK 99709, USA

15

16 Corresponding author: Claudine Hauri (chauri@alaska.edu)

Abstract

Warming, ocean acidification, and deoxygenation are increasingly putting pressure on marine ecosystems. At the same time, thawing permafrost and decomposing hydrates in Arctic shelf seas may release large amounts of methane (CH_4) into the water column, which could accelerate local ocean acidification and contribute to climate change. The key parameters to observing and understanding these complex processes and feedback mechanisms are vastly undersampled throughout the oceans. We developed carbon dioxide (CO_2) and CH_4 gliders, including standard operational procedures with the goal that CO_2 and CH_4 measurements become more common for glider operations. The Seagliders with integrated Contros HydroC CO_2 or CH_4 sensors also include conductivity, temperature, depth, oxygen, chlorophyll-a, backscatter, and fluorescent dissolved organic matter sensors. Communication via satellite allows for near-real time data transmission, sensor adjustments, and adaptive sampling. Several sea trials with the CO_2 Seaglider in the Gulf of Alaska and data evaluation with discrete water and underway samples suggest near 'weather quality' CO_2 data as defined by the Global Ocean Acidification Network. A winter mission in Resurrection Bay, Alaska provided first insights into the water column inorganic carbon dynamics during this otherwise undersampled season. The CH_4 Seaglider passed its flight trials in Resurrection Bay, yet needs to be tested during a field mission in an area with CH_4 concentrations beyond background noise. Both sensing systems are available to the science community through the industry partners (Advanced Offshore Operations and -4H-JENA engineering GmbH) of this project.

1. Introduction

39   Understanding the distribution and dynamics of carbon dioxide (CO_2) and methane (CH_4)

40   in the ocean is crucial for predicting and mitigating climate change and ocean acidification

41   impacts. Within the ocean, CO_2 levels (measured as the partial pressure of CO_2, pCO_2 and/or

42   fugacity of CO_2) are spatially and temporally variable as they are influenced by a myriad of

43   highly dynamic physical, chemical, and biological processes. On top of this natural variability,

44   the ocean has absorbed about one third of the CO_2 emitted by humans since the industrial

45   revolution (Sabine et al., 2004; Gruber et al., 2019). In doing so, it has played an important role

46   in mitigating climate change (Sabine and Tanhua, 2010). However, both the oceanic uptake of

47   anthropogenic CO_2 and climate change are altering the distribution of oceanic CO_2 and are

48   causing ocean acidification (Doney et al., 2009; Qi et al., 2022; Woosley and Millero, 2020). At

49   the same time, the oceans are warming and losing oxygen (Johnson and Lyman, 2020; Breitburg

50   et al., 2018), increasing the stress on marine ecosystems. As these long-term changes unfold,

51   marine heat waves, and high acidity or low oxygen extreme events will last longer, become more

52   intense, and happen more often and at the same time (Laufkötter et al., 2020; Gruber et al., 2021;

53   Hauri et al., 2024). Negative effects on certain organisms are even stronger if exposed to a

54   combination of different stressors (Breitberg et al., 2015; Kroeker et al., 2017).

55   Over 100 years, CH_4 possesses a global warming potential approximately 28 times

56   greater than that of CO_2 (IPCC AR5; Myhre et al., 2013). Sediments along the seafloor at

57   continental margins contain large amounts of CH_4, with about ten times as much carbon as the

58   atmosphere (Kessler, 2014). CH_4 is biologically produced in anoxic sediments and the surface

59   mixed layer or released from geological sources like hydrocarbon seeps and degrading methane

60   hydrate deposits (Barnes and Goldberg; Du et al, Skarke 2014). This powerful greenhouse gas is

61   emitted to the atmosphere through bubbling (ebullition) or diffusive gas transfer (Reeburgh,

3

62   2007; McGinnis et al., 2006), which is limited by rapid oxidation to CO_2 during transport

63   through the water column (Leonte et al., 2017). CH_4 occurs generally at low levels (background

64   concentrations) throughout oceans, unless close to a source. Positive feedback mechanisms, like

65   warming induced CH_4 seepage from destabilizing hydrates and thawing subsea permafrost, may

66   further accelerate ocean acidification and climate change (Garcia-Tigreros et al., 2021; Sparrow

67   et al., 2018; Shakhova et al., 2010; Rees et al., 2022).

68   To effectively observe and understand the complex processes and feedback mechanisms

69   regulating Earth's systems, certain key parameters, defined by the Global Ocean Observing

70   System as essential ocean variables, must be measured accurately. However, these variables are

71   often vastly undersampled across time and space due to traditional sampling methods, which rely

72   mainly on discrete water sample collections from dedicated research cruises, underway

73   measurements from transiting vessels, or time series measurements from in situ sensors on fixed

74   moorings. Although biogeochemical sensors deployed on autonomous platforms like moorings

75   and Argo floats have become more prevalent, challenges such as high power requirements,

76   sensor size, and data quality hinder their widespread use on underwater gliders. Autonomous,

77   spatially resolved surface measurements of $p\mathrm{CO}_2$ and pH are collected using wave gliders and

78   sail drones (Chavez et al., 2018; Nickford et al., 2022; Manley and Willcox, 2010). The state-of-

79   the-art biogeochemical (BGC) Argo floats measure variables like pH, O_2, NO_3, chlorophyll-a,

80   suspended particles, and downwelling irradiance in subsurface waters (Claustre et al., 2020).

81   These floats can last several years at low sampling resolutions, such as a 2000-meter depth

82   profile every ten days, or they can be programmed for high-resolution and shallow sampling.

83   They can even sample beneath seasonal sea ice (Briggs et al., 2018). Despite their capabilities,

84   their trajectory is hard to control, and they are usually not recovered after their mission, which

85   prevents sensor calibration and post-mission corrections.

86   Ocean gliders autonomously collect water column data along planned waypoints, which

87   allows for controlled exploration and adaptive sampling. To date, pH is the only carbon system

88   parameter that has been successfully integrated into ocean gliders (Hemming et al., 2017; Saba et

89   al., 2019; Possenti et al., 2021; Takeshita et al., 2021). The most promising results came from

90   ISFET based pH sensors (Saba et al., 2019; Wright-Fairbanks et al., 2020; Takeshita et al.,

91   2021). However, ISFET-based pH sensors require significant conditioning periods before

92   deployment, suffer from biofouling, require annual cleaning and calibration at the manufacturer,

93   and careful discrete sample collection at deployment and recovery to characterize and correct for

94   sensor drift (Thompson et al., 2021). There have been few attempts to integrate pCO_2 sensors

95   into gliders (Hemming et al., 2017; Hauri et al., 2018; von Oppeln-Bronikowski et al., 2021).

96   Hemming et al. (2017) did not publish the data because of low quality. Von Oppeln-Bronikowski

97   et al. (2021) integrated an Aanderaa CO_2 optode that measures pCO_2 by detecting the

98   luminescent quenching response from a CO_2-sensitive membrane with a Slocum G2 glider but

99   suffered from instability, thermal-lag issues, variable conditioning periods (4 days to 1 month),

100 large offsets (> 1000 uatm), nonlinear temperature-dependent response time, and a high

101 dependence on prior foil calibration. Hauri et al. (2018) integrated the Pro Oceanus Mini Pro

102 CO_2 sensor with a Slocum G2. However, the Pro Oceanus Mini Pro CO_2 sensor used at the time

103 did not withstand the pressure changes imposed by glider missions. The Franatech METS CH_4

104 sensor has been integrated into Alseamar SeaExplorer and Teledyne Slocum gliders and

105 successfully used to generate concentration maps of a methane seep in a semi-quantitative way

106 (Meurer et al., 2021).

107   Here we integrated modified versions of the Contros HydroC CO_2 and CH_4 sensors with

108   a Seaglider® (registered trademark of the University of Washington). We discuss details of the

109   physical and software integration, present CO_2 and CH_4 data from tank experiments, evaluate the

110   quality of $p$$CO_2$ data collected during CO_2 Seaglider missions, and discuss highlights from

111   missions in Resurrection Bay, Alaska.

112

113   **2. Methods**

114   2.1 CO_2 Seaglider

115   We integrated a modified version (Seaglider (SG) HydroC CO_2) of the CONTROS

116   HydroC^{TM} CO_2 sensor (-4H-JENA engineering GmbH, Kiel, Germany) with a Seaglider M1

117   (Figure 1 a and b). The Seaglider M1 was specifically designed for long endurance missions in

118   deep waters to 1000 m depth. The HydroC CO_2 sensor was outfitted with a semi-permeable

119   TOUGH membrane (Pinnau and Toy, 1996) that equilibrated dissolved CO_2 between the ambient

120   seawater and the headspace of the sensor, where the gas concentration was determined by

121   nondispersive infrared (NDIR) spectrometry.

122   Since the equilibration time (response time) of membrane-based sensors is affected by the

123   exchange of the water mass in front of the sensor head, we installed a Seabird Electronics (SBE)

124   5M pump next to the SG HydroC CO_2 sensor using tubing to transfer seawater from outside the

125   glider fairing to the membrane surface (Figure 1a). The response time was determined at the

126   manufacturer, verified in the field, and then used to correct for hysteresis during the post-

127   processing phase (see Section 2.7.2).

128   The form factor of the HydroC CO_2^{TM} sensor and Seaglider were changed to achieve an

129   internal integration of the sensor with the Seaglider. The standard high-performance HydroC

130   CO_2^{TM} sensor was changed from ⌀ 89 x 380 mm to ⌀ 136 x 294 mm by rearranging the gas-cycle

131   components and the control unit (Figure 1c). This new SG HydroC CO_2 sensor is available in

132   polyoxymethylene (POM) cladding rated to 300 m or a titanium housing rated to 1000 m to

133   provide a choice between a coastal mission and an offshore deeper mission. Use of the titanium

134   housing required a syntactic foam housing to compensate for the weight, whereas the POM

135   housing was integrated into the glider with simple brackets (Figure 2). Despite these adjustments

136   to the size of the sensor, to our knowledge, it is still the largest and heaviest sensor that has been

137   integrated with a Seaglider to date. The forward fairing of the Seaglider was extended by 40 cm

138   with a fiberglass cylindrical extension to create internal wet payload space for the sensor, pump,

139   and cables (Figure 1 a and b). The sensor was mounted with the membrane facing aft to ensure

140   that potential bubbles within the internal tubing of the sensor could escape the system during the

141   downcast of the first dive. In situ comparison of the orientation of the sensor and close

142   examination of pCO_2 and internal pressure data suggested the highest data quality was achieved

143   with this mounting design.

144   One of the advantages of using ocean gliders for ocean observing is the ability for real-

145   time communication of data and commands between the pilot and the glider. To take advantage

146   of this, modifications were needed to allow two-way communication between the Seaglider

147   firmware and the HydroC firmware. The Seaglider firmware has a feature to allow easy

148   integration of "logging devices," which provides a way to build commands for the pilot on land

149   to switch the sensor on and off and change sampling strategy during the mission (on/off below or

150   above certain depth) when it comes to the surface for a communication session. The Seaglider

151   firmware can also automatically set the clock of the sensor on request at every surfacing and

152   send small samples of the data stream via Iridium along with the standard sensor data. This

7

153 required the writing and testing of a driver file (CNF file). However, to take full advantage of the

154 ability of the HydroC, a more-advanced electronic integration was carried out using Smart

155 Interoperable Real-time Maritime Assembly (SIRMA™, registered trademark of Cyprus Subsea

156 Consulting and Services, C.S.C.S., Ltd.). This small programmable electronic circuit contained

157 hardware elements to adapt the sensor power and communication requirements to those available

158 on the host platform. It also allowed for separate storage and processing capabilities to

159 supplement the main host processor that controls the flight, sampling, and telecommunications of

160 the host. Most importantly here, it was programmed to relay pilot commands to the SG HydroC

161 CO_2 for the built-in "zero" function, which isolated the internal gas circuit until there was no

162 CO_2 present, measured the concentration signal, and assigned a zero value. Then the gas circuit

163 was exposed to the headspace behind the diffusion membrane for in situ sampling. SIRMA was

164 also programmed to extract raw data from the HydroC and calculate the bin average of some of

165 the output fields, which were useful for real-time mission adaptation and confirmation of sensor

166 operation. Three levels of output were allowed, depending on how much surfacing time could be

167 tolerated before continuing the mission (Baud rate for Iridium is very low, on the order of 4800

168 bps). More detailed information can be found in the CO_2 Seaglider SOP (Irving et al., 2024).

169   In addition to the HydroC CO_2 sensor, the CO_2 Seaglider carried an Aanderaa 4831F

170 optode, a compact optical oxygen sensor, which works on the principle of luminescence

171 quenching by oxygen. The 4831F was equipped with a fast response sensing foil with a well-

172 characterized response time of 8 seconds. The Aanderaa optode measured absolute oxygen

173 concentration and percentage saturation. It is the most widely used on ocean gliders and has been

174 integrated into both Slocum and Seagliders (OceanGliders Oxygen SOP, 2024; Bittig et al.,

175 2018). The OceanGliders community has developed a Standard Operating Procedure (SOP) that

176 details everything from mounting, calibration, available sensors, piloting tips, and response time

177 correction, to post-processing (OceanGliders Oxygen SOP, 2024). The CO_2 Seaglider was also

178 outfitted with an SBE CT sail and Wetlabs Ecopuck measuring chlorophyll fluorescence at 695

179 nm.

180

181 **2.2 CH_4 Seaglider**

182 We also integrated a modified version of the CONTROS HydroC CH_4 sensor (-4H-JENA

183 engineering GmbH, Kiel, Germany) with the Seaglider. The manufacturer's published

184 uncertainty of the HydroC CH_4 sensor is 2 µatm or ± 3 %, whichever is greater . The SG HydroC

185 CH_4 sensor had the same form factor as the SG HydroC CO_2 sensor. However, it was 0.5 kg

186 heavier due to its Tunable Diode Laser Absorption Spectroscopy (TDLAS) component, so the

187 SG HydroC CH_4 had to be integrated with changes to the glider's ballast.

188

189 **2.3 Spring and winter CO_2 Seaglider missions**

190 Both versions of the CO_2 Seaglider (rated to 300 m versus 1000 m) were tested in

191 separate missions (Figure 3, Table S1) in spring (53 dives, May 4 – 7, 2022, Figure 5) and winter

192 (310 dives, February 8 – 21, 2023, Figure 6). The 300 m version with integrated POM housing

193 was tested during a five-day-long mission in May 2022. The glider followed along a transect

194 within Resurrection Bay. CTD casts near the glider path allowed for in-depth evaluation of the

195 data quality. The 1000 m depth-rated CO_2 Seaglider with integrated titanium housing was tested

196 in February 2023. Estimated energy consumption during the CO_2 Seaglider missions was 19 out

197 of 135 Ah and 75 out of 120 Ah for the 24 V which powered the SG HydroC CO_2 sensor battery

198 for the spring and winter missions, respectively. Before the February mission, the on board

199   modem was replaced with a newer model, with different input voltage requirements, which were

200   probably not met as the mission evolved. As a result, the glider could not communicate and was

201   lost. While this was an unfortunate mistake, the loss of the glider had nothing to do with the

202   HydroC CO_2 integration.

203

204   **2.4 Tank experiments**

205   Shortly before the May 2022 glider mission, the glider was kept in a flow-through tank at

206   the Alutiiq Pride Marine Institute for roughly 12 h for cross-calibration purposes. The flow-

207   through tank was fed with water from about 75 m depth and 91 m from the laboratory into

208   Resurrection Bay, near a freshwater source. During the tank experiment, SG HydroC CO2T-

209   0718-001 (Figure 4b, blue line) was integrated into the Seaglider, and SG HydroC CO2T-0422-

210   001 (Figure 4b, black line) and the SG HydroC CH_4 (Figure 4c) sensors were secured next to the

211   Seaglider. The water was kept in motion with a circulation pump. Triplicate discrete water

212   samples for dissolved inorganic carbon, pH, and CH_4 analysis were taken every four hours

213   (Table 1).

214

215   **2.5 Rosette package**

216   One of the SG HydroC CO_2 sensors (CO2T-0422-001) was installed on an SBE-55 frame

217   ECO water sampler with six 4-liter sample bottles (Seabird Scientific) during the May 2022 trials

218   (Tables 2 and 3, Figure 7 and S1). The SBE-55 and SG HydroC CO_2 were powered by an SBE-

219   33 carousel deck unit. The SG HydroC CO_2 interfered with the communication stream and

220   thereby prevented real-time data acquisition and control of the SBE-55, however data were

221   internally logged. The depth of the rosette package was monitored directly on the winch and the

222   timing of firing of the sample bottles, after an approximate 15-minute hovering period (to allow

223   for equilibration), was programmed in advance based on time intervals. On May 3 (Table 2,

224   Figure 7) only samples from the upper 20 m of the water column were usable due to issues with

225   manually measuring the depths and the sample collection. On May 7 (Table 3, Figure S1) two

226   bottles that were intended to be fired while the rosette was stationary at depth, were instead fired

227   while the rosette was in motion.

228

229   **2.6 Discrete water samples**

230   2.6.1 Inorganic carbon chemistry

231   Discrete seawater samples were collected for sensor validation in two different cases in

232   May of 2022. Firstly, samples were taken alongside two SG HydroC CO_2 sensors during a tank

233   experiment at the Alutiiq Pride Marine Institute (Figure 4b, Table 1), from adjacent sample

234   bottles (Figure 1d). Secondly, samples were taken from bottles during a CTD cast within 1 km

235   and 4 hours of the HydroC measuring pCO_2 on the glider while conducting dives (Section 3.2).

236   Inorganic carbon sampling in the Gulf of Alaska's glaciated coastal regions required

237   methodological variations from open-ocean best practices to ensure that suspended mineral

238   particles do not compromise the instrumentation and/or bias measurements between sample

239   collection and analysis (Sejr et al., 2011). Given this, the discrete seawater samples were filtered

240   (replaceable 0.45 µm filter in a 47 mm polycarbonate in-line filter) with a peristaltic pump

241   straight from the Niskin bottles (see Bockmon and Dickson (2014) for detailed method), or tank,

242   into pre-cleaned 500 mL borosilicate bottles, and poisoned with 200 µL mercuric chloride

243   ($HgCl_2$) (Dickson et al., 2007). Samples were transported and stored at room temperature before

244   analysis. Samples were opened immediately (< 10 minutes) before concurrent analyses of pH

245   and DIC to limit gas exchange with ambient lab conditions. Samples were analyzed for DIC

246   using an Apollo SciTech, LLC Dissolved Inorganic Carbon Analyzer model AS-C6. All species

247   of dissolved inorganic carbon in a sample were converted to CO_2 by the addition of a strong acid.

248   The CO_2 gas was then purged from the sample through a drying system. The concentration of

249   CO_2 gas was measured using a non-dispersive infrared gas analyzer, the LI-7000 CO_2/H_2O

250   Analyzer. This method required Certified Reference Material (CRM, Batch #198 from A.

251   Dickson's Certified Reference Materials Laboratory) to create a three-point calibration line. The

252   calibration line was used to quantify the total amount of CO_2 in the sample as the integrated area

253   under the concentration-time curve. Apollo SciTech recommendations to improve analytical

254   accuracy were followed and included bubbling of CO_2 off the acid daily, allowing the analyzer to

255   warm up for at least 2 hours before measurements begin, measuring a set of standards at the

256   beginning and end of each day and every 9 samples, using Ultra High Purity (UHP) N_2 gas, and

257   filtering the N_2 gas with a PTFE filter, CO_2 scrubber (Ascarite II) and H_2O scrubber

258   $(Mg(ClO_4)_2)$.

259   Samples were analyzed spectrophotometrically for pH with a CONTROS HydroFIA pH

260   (Aßmann et al., 2011) operating in discrete measurement mode using unpurified m-Cresol Purple

261   (mCP) as the indicator dye (Clayton and Byrne, 1993). Sample temperature was stabilized at

262   25C+/-0.01 during measurements using Peltier elements and 5 repetitive measurements were

263   taken for each sample. At the beginning of each day, the HydroFIA pH underwent a conditioning

264   period using seawater with similar properties until values stabilized. CRMs (known TA and DIC

265   concentration, Batch #198 from A. Dickson's Certified Reference Materials Laboratory) were

266   measured at the beginning and end of the day, as well as every 9 samples.

267   All data processing and analyses were done using an in-house MATLAB routine. In situ

268   pH and pCO_2^{disc} were calculated from input pair pH_{lab} and DIC using CO2SYSv3 (Sharp et al.,

269   2023) with dissociation constants for carbonic acid of Sulpis et al. (2020), bisulfate of (Dickson,

270   1990), hydrofluoric acid of Perez and Fraga, (1987), and the boron-to-chlorinity ratio of (Lee et

271   al., 2010). Sulpis et al. (2020) found that the carbonic acid dissociation constants of Lueker et al.

272   (2000) may underestimate pCO_2 in cold regions (below ~8°C) and, therefore, overestimate pH

273   and CO_3^{-2}. Differences between discrete pCO_2 calculated with the carbonic acid dissociation

274   constants by Lueker et al. (2000) (the standard in synthesis data products (e.g., Jiang et al., 2021,

275   Lauvset et al., 2022, Metzl et al., 2024) and the HydroC pCO_2 from the tank experiment were

276   found to be on average 4.6 μatm (1.6 %) and 4.2 μatm (0.7 %) greater for SN0422 and SN0718,

277   respectively, when compared with discrete pCO_2 based on carbonic acid dissociation constants

278   by Sulpis et al. (2020).

279   Discrete pCO_2 uncertainty (u_c) was calculated as the combined standard uncertainty from

280   *errors.m* (Orr et al., 2018) that propagates input uncertainties. Input uncertainties for pH_{lab} and

281   DIC were the standard uncertainties, defined as the square root of the sum of the squared random

282   uncertainty component plus the squared systematic uncertainty components. For pH_{lab} the

283   random uncertainty was the sample precision, or standard deviation of the measurements. For

284   DIC, the random uncertainty was the propagated error calculated with the first-order Taylor

285   series expansion (Equation 1, Orr et al. (2018)) and assuming the correlation term was zero for

286   the conversion of molarity (μmoles l^{-1}) to molality (μmoles kg^{-1}). Systematic uncertainty

287   components were the uncertainty in the CRM used for instrument offset and drift correction, and

288   the published instrument accuracy, or if available, the daily instrument accuracy as defined

289   below. Daily instrument accuracy was defined as the maximum difference between the known

290   CRM concentration, and the measured CRM concentration after data were corrected for

291   instrument drift and offset of all available CRM's not used in the instrument drift and offset

292   calculation. CRM pH_{lab} "known" values were calculated using CO2SYSv3 (Sharp et al., 2023)

293   with inputs pH and DIC. Nutrient concentrations (SiO_4^{-2}, PO_4^{-3}) were assumed to be negligible in

294   the CO2SYS calculations (e.g. DeGrandpre et al., 2019; Vergara-Jara et al., 2019; Islam et al.,

295   2017).

296

297   2.6.2 Methane

298   Two sets of triplicate pCH$_4$ discrete water samples were collected during the tank

299   experiment for an initial evaluation of the SG HydroC CH$_4$ sensor (Figure 4c, Table 1). Seawater

300   was filtered from the tank into 250 mL vials. The vials were closed with a rubber stopper, topped

301   with an aluminum cap, and closed with a crimp immediately. A dry and clean syringe was

302   flushed with 10 mL of N$_2$ gas twice. The third fill was kept, and the syringe valve was closed. N$_2$

303   was then injected into the headspace while simultaneously pulling 10 mL seawater out of the vial

304   using a second syringe. 50 µL mercuric chloride (HgCl$_2$) were added to the vial, which was then

305   shaken for about a minute and put into a fridge at 4°C for over 12 h to equilibrate the headspace.

306   The samples were then sent to the Kessler analytical laboratory at the University of Rochester for

307   analysis.

308

309   **2.7 Data post-processing**

310   *2.7.1 pCO$_2$ post-processing*

311   SG HydroC CO$_2$ data were post-processed using Jupyter Notebook scripts developed by -4H-

312   JENA engineering GmbH at the original resolution (2 seconds). SG HydroC CO$_2$ (SG HydroC

313   CO2T-0422-001) data from the tank experiment (Table 1, Figure 4) and rosette mounted CTD

314   casts (Table 2 and 3, Figure 7 and S1) were post-processed to correct for baseline drift (change in

315   the zero signal reference) and span drift (changes in the sensor's concentration dependent

316   characteristics) using pre- and post-calibration coefficients interpolated over the

317   deployment (Fietzek et al., 2014). For the May 2022 Seaglider integrated SG HydroC

318   CO_2 sensor (SG HydroC CO2T-0718-001, Table 3, Figures 8 and 9), data were post-processed

319   with pre-calibration coefficients only (no span drift correction) because the sensor was damaged

320   during the return shipment for post-calibration. Differences between sensors remained low

321   despite the difference in processing, with a mean difference during the tank experiment of 2.1 ±

322   1.0 μatm (0.9%) and median difference of 2.0 ± 1.0 μatm (0.9%) (Table 1, Figure 4b).

323   The pCO_2 data from February 2023 was collected with a sensor that was factory calibrated two

324   weeks prior to deployment (SG HydroC CO2T-0422-001) but were not post-processed because a

325   required parameter (*p_NDIR*) was not relayed in real-time and the glider was lost. Lack of post-

326   calibration most likely had no negative effect on the quality of data since the HydroC was only

327   collecting data for ~4 days during the spring mission and ~2 days during the winter mission.

328   HydroC pCO_2 and pCO_2^{RTC} data at the original resolution (2 s) and RTC resolution (8 s)

329   were linearly interpolated onto the Seaglider timestamp and 1-meter binned data were calculated

330   by first averaging 1 meter (+/- 0.5 m) upcast and downcast data independently, linearly

331   interpolating over gaps, then averaging the interpolated 1-meter binned upcast and downcast

332   together.

333

334   *2.7.2 Response time correction*

335   The ability to determine the in situ response time (τ_{63} of the HydroC, which took into

336   account membrane characteristics and the rate of water exchange over the membrane, i.e.

337   pump characteristics) of the sensor made correction for hysteresis through data post processing

338   possible. This is critical for a sensor operating on profiling platforms, especially in the Gulf of

339   Alaska, where strong environmental gradients were encountered. Fiedler et al. (2013) used a

340   CONTROS HydroC^{TM} CO_2 with a silicone, polydimethylsiloxane (PDMS) membrane and

341   reported a linear response time dependency on water temperature on the order of one second per

342   one °C. For this study, the SG HydroC CO_2 sensors were deployed with the new robust TOUGH

343   membrane, which had Teflon AF2400 as the active separation layer with a low temperature

344   dependence on the permeability coefficient (Pinnau and Toy, 1996). Response times determined

345   during calibration at -4H-JENA were used for response time correction (RTC) and found to be

346   106 seconds for the HydroC mounted on the rosette in May 2022 and 108 seconds when it was

347   integrated into the Seaglider in February 2023 (HydroC CO2T-0422-001). The response time of

348   the HydroC integrated into the Seaglider in May 2022 (HydroC CO2T-0718-001) was 109

349   seconds. Since field verification of the response time was recommended to ensure the highest

350   quality post-processed data product (because τ_{63} can be affected by the speed of water exchange

351   across the membrane (e.g. pump speed, tube length, etc.)), we verified the sensor response time

352   at deployment. After the glider was stationary for approximately 15 minutes, a zeroing interval

353   was performed with the HydroC CO_2. The response time was determined by reviewing the time

354   it took for the signal to recover to the ambient concentration. Our in situ response time tests were

355   suggested to be within 5 seconds of the response time found during calibration (not shown).

356   Before RTC was applied, HydroC CO_2 data were smoothed using a quadratic regression

357   (MATLAB's smoothdata.m function with the loess method) over a 2-minute window. This was

16

358   done to eliminate erroneous spikes in the RTC signal while retaining the original 2-second

359   resolution of the pCO_2 data. The RTC resolution of 8 seconds was determined with the L-curve

360   analysis included in the publicly available code from Dølven et al. (2022). The Dølven et al.

361   (2022) RTC method was used because it produced more realistic profiles than an RTC method

362   (Miloshevich et al., 2004, not shown) previously used for HydroC CO_2 correction from a

363   profiling float (Fielder et al. 2013). In addition, Dølven et al. (2022) developed their algorithm

364   with equilibrium-based sensors in mind and was proven with a sensor with a long response time

365   (HydroC CH4 $\boldsymbol{\tau}63 \cong 23$ minutes).

366

367   *2.7.3 pCH4 post-processing*

368   SG HydroC pCH_4 data were response time corrected using a τ_{63} of 43 minutes (Dølven et

369   al., 2022; Figure 4c, blue line). Before RTC was applied, HydroC CH_4 data were smoothed using

370   a quadratic regression (MATLAB's smoothdata.m function with the Loess method) over a 2-

371   minute window to avoid erroneous spikes in the RTC data while retaining the original 2-second

372   resolution of the pCH_4 data. The RTC resolution of 30 seconds was determined with the L-curve

373   analysis included in the publicly available code from Dølven et al. (2022). Discrete CH_4 samples

374   were collected during the tank experiment (Table 1; Figure 4c red diamonds) and analyzed at

375   John Kessler's laboratory at the University of Rochester. Discrete CH_4 sample values were

376   converted from the concentration of dissolved gas in water (mol L^{-1}) to partial pressure (pCH_4^{disc},

377   μatm) using the solubility coefficient following Sarmiento and Gruber (2006). pCH_4^{disc}

378   uncertainty (u; Table 1; Figure 4c red error bars) was calculated as the square root of the sum of

379   the squared 1) mean of the standard deviations from each sample as returned from the lab and 2)

380   the standard deviation of the triplicates.

381

3. Results

3.1 Glider flight

Despite the large payload and major changes to the vehicle fairing, the glider was able to "fly" properly, allowing the desired undisturbed flow to meet the sensor's requirements. Example flight profiles with the POM and Titanium integrated sensors are shown in Figures 5 and 6, respectively. Pitch and vertical velocity are in the stable range, and roughly symmetric between downcast and upcast, indicating a nearly balanced glider. Heading varies around the targeted value as the roll adjusted to heading errors. It should be noted that this level of variability is typical of standard Seagliders. Operating Seagliders in shallow water (< 200 m) is risky because of the likelihood of meeting depth-averaged currents of the same order of magnitude as the vehicle speed. A typical single dive cycle of downcast and upcast shows that the sensor data are free of noise that could be expected if there were recirculated water from the glider meeting the sensors. The expected endurance of the CO_2 Seaglider is around 18 days and 15 days for the CH_4 Seaglider with constant sampling at full depth.

3.2 CO_2 Seaglider data evaluation

The quality of the CO_2 Seaglider data was thoroughly tested with discrete measurements during a tank experiment, nearby CTD cast, and glider missions.

3.2.1 Tank experiment

Discrete water samples show good agreement with the SG HydroC CO_2 sensors (Figure 4b, Table 1). The values of discrete water samples represent the average of triplicate samples

18

404   (Figure 4c, red diamonds). Differences between the SG HydroC CO_2 sensors remained low, with

405   a mean difference during the tank experiment of 2.1 ± 1.0 µatm (0.9 %) and median difference of

406   2.0 µatm (0.9 %; Table 1). Percent differences (Eq. 1) between the SG HydroC CO_2 sensors and

407   discrete water samples collected in the tank were between 0.3 and 1.9 % (Table 1, Figure 4).

408    $\% \; difference \; = \frac{|pCO_2{}^{HydroC} - pCO_2{}^{disc}|}{(pCO_2{}^{HydroC} + pCO_2{}^{disc})}/2 * 100\%$ (Equation 1)

409

410   3.2.2 Profiling experiment

411   Rosette-based profiles with the SG HydroC CO_2 sensor in combination with discrete

412   water samples were used to test and evaluate the response correction algorithm by Dølven et al.

413   (2022). The rosette was lowered into the water and kept at different depths for about 20 minutes

414   at a time (Figure 7a and Figure S1a). Sample bottles were programmed to collect seawater

415   toward the end of each hovering period. pCO_2 measured with the HydroC ranged from 218 µatm

416   at the surface to 411 µatm at 80 m depth on May 3 (Figure 7b) and 231 µatm at the surface to

417   382 µatm at 77 m depth on May 7 (Figure S1). Differences between the rosette mounted SG

418   HydroC CO_2 sensor and discrete samples ranged from -3.3 µatm (1.4 %) to 8.2 µatm (3.4 %)

419   with a lowest percent difference of 0.6 % (Table 2) on May 3 and from -5.7 µatm (1.6 %) to 12.1

420   µatm (3.8 %) with a lowest percent difference of 0.3 % (Table 3) on May 7.

421

422   3.2.3 Data evaluation during CO_2 Seaglider mission

423   The quality of the pCO_2 data from the CO_2 Seaglider was further evaluated during a 3-

424   day long sea trial mission in spring 2022 in Resurrection Bay, Alaska (Figure 3).

425   Discrete water samples were taken in proximity (1 km and within 4 hours) of the downcast of

426   dive #51 (Figures 8 and 9a, Table 3). The response time corrected CO_2 Seaglider data compares

427   well with the discrete water samples (Figure 8), overestimating the discrete water samples

428   between 8.3 µatm (2.6 %) and 12.0 µatm (5.0 %) (Table 3). The mean difference between the

429   rosette mounted and Seaglider integrated SG HydroC CO_2 sensors during the May 7th cast at the

430   time of discrete samples was 8.5 µatm +/- 8.9 µatm (3.7 %). The larger difference between SG

431   HydroC CO_2 sensors compared to the difference during the tank experiment (see Section 3.2.1)

432   is unsurprising, given the spatial and temporal distance between sensors (Table 3). Collecting

433   more discrete samples throughout the water column and in closer proximity (within 100 m,

434   Thompson et al., 2021) to the CO_2 Seaglider conducting dives would allow a more tightly

435   constrained uncertainty estimate for response time corrected pCO_2 data collected on a glider and

436   should be a priority for future researchers.

437

438   **3.3 CH_4 Seaglider data evaluation**

439   3.3.1 Tank experiment

440   The SG HydroC **CH_4** was also evaluated during the tank experiment described in section

441   2.4 (Figure 4c). Percent differences (Eq. 1) between discrete pCH_4 (average of triplicate samples)

442   and pCH_4^{RTC} were 6.3 to 14.6 % (Table 1). During the experiment, there was a decrease in

443   salinity from 30.95 to 29.88 where pCO_2 decreased by 80 µatm. The corresponding pCH_4^{RTC}

444   signal decreased by 25.4 µatm from 32.3 to 6.9 µatm. Although the triplicate discrete pCH_4 water

445   samples were slightly lower than the sensor-measured pCH_4 values, they also reflected this step

446   change.

447

3.4 Winter and springtime pCO_2 in Resurrection Bay, Alaska

The surface-to-subsurface pCO_2 gradient is much larger in spring than in winter (Figure 10). During the early May mission, the average surface $pCO_{2,Seaglider}^{RTC}$ was 240.7 +/- 16.5 µatm (mean +/- standard deviation at 2 meters) with an average temperature of 5.8 +/- 0.4 °C (Figures 9 and 10). In February, surface $pCO_{2,Seaglider}^{RTC}$ was near atmospheric pCO_2 (427.4 +/- 13.0 µatm, temperature 4.1 +/- 0.3 °C) and about 180 µatm higher than in May (Figures 10 and 11). NOAA's moored sensor located in Sunny Cove (59.911 °N, -149.35 °W), near the CO_2 Seaglider trial site, measured an average sea surface pCO_2 of 240.7 +/- 10.4 µatm during the time of the May 2022 mission (Monacci et al., 2023), which compared remarkably well with the Seaglider based measurements. A minimum of 140 µatm was measured in Sunny Cove in mid-April (3-day average) (Figure 12, Monacci et al., 2023), suggesting that the peak of the spring bloom happened three weeks before the May 2022 glider mission. Since we don't have salinity data from the May CO_2 Seaglider mission (conductivity sensor failure), we cannot disentangle the contributions of freshwater or primary production on the low surface pCO_2 values observed (Figure 9). The moored sensor in Sunny Cove measured an average sea surface pCO_2 of 416.4 +/- 4.2 µatm during the time of the February mission, straddling the atmospheric pCO_2 values (Monacci et al., 2023, Figure 12). Subsurface $pCO_{2,Seaglider}^{RTC}$ at 180 m was on average 545.6 +/- 16.9 µatm during the February mission and 518.2 +/- 37.4 µatm during the May 2022 mission (Figure 10a). pCO_2 was much lower in May than in February throughout the upper water column (< 120 m), whereas there was not much of a seasonal difference at deeper depth. Some of the fine scale features apparent in the May pCO_2 and O_2 profiles are likely due to various levels of photosynthetic activity (Figure 10). As the glider transitioned into the open Gulf of Alaska during the February mission, water with O_2 < 150 µM shoaled into the upper 150 m of the water

21

471   column (Figure 11). Unfortunately, the HydroC CO_2 sensor was turned off at that stage of the

472   mission to conserve battery.

473

474   **4. Discussion**

475   The newly developed CO_2 Seaglider is the first of its kind to autonomously collect high

476   quality pCO_2 data. The tank and rosette experiments and in situ data evaluation suggest that the

477   post-processed data from the CO_2 Seaglider generally fall near the relative uncertainty of 2.5%,

478   which is a threshold defined as the "quality sufficient to identify relative spatial patterns and

479   short-term variation" ("weather quality", Newton et al., 2015). This is the highest quality of

480   pCO_2 data that has been measured with a subsurface autonomous vehicle to this date and

481   therefore an important step towards filling the subsurface carbonate system data gap. -4H-JENA

482   is reassessing their sensor calibration methodology and data post-processing algorithm to further

483   improve the HydroC's data accuracy.

484   The newly developed CO_2 Seaglider is suitable for data collection in open ocean or

485   coastal environments with bottom depths deeper than 300 m. However, the coastal Gulf of

486   Alaska is a highly dynamic environment, with strong freshwater and wind influence, and rugged

487   shallow (often < 200 m) bottom topography. Strong currents (up to 0.50 m s^{-1}) made the piloting

488   of the glider extremely difficult throughout the project and confirmed that the Seaglider cannot

489   reliably reach desired waypoints in these conditions. The current version of the CO_2 Seaglider is

490   also not suitable for operating in the coastal Gulf of Alaska in summer and early fall, due to

491   strong seasonal salinity gradients in this freshwater influenced area. Another issue we faced was

492   the fact that the forward-looking altimeter could not detect the Seafloor as it should in its

493   position behind the HydroC CO_2. In areas with detailed topography maps this would not be an

494   issue, but in the coastal Gulf of Alaska reliable topography information is not readily available

495   yet. An obvious next step is to integrate the SG HydroC CO_2 sensor into a newer glider platform,

496   such as the Seaglider SGX or Teledyne Slocum G3 glider. The extended energy bay, larger

497   buoyancy range, and thruster should make the operation of the coastal Slocum G3 with HydroC

498   sensors relatively easy and would allow for autonomous high-resolution water column

499   measurements of pCO_2 and pCH_4 in dynamic coastal environments. The integration of a HydroC

500   on a Slocum glider will require a custom-made wet-payload bay due to the size of this sensor.

501   For open ocean or deeper coastal regions, the integration with the Seaglider SGX, with 60%

502   higher energy capacity, would be effective and nearly identical to the work already done here.

503   The SG HydroC CH_4 was successfully integrated into the Seaglider as part of this project.

504   While tank experiments showed promising results, short field tests of the CH_4 Seaglider in

505   shallow water revealed low and patchy methane concentrations near the detection limit (not

506   shown). The CH_4 Seaglider requires further testing in environments with strong pCH_4 gradients

507   during longer and deeper dives (to allow for equilibration) to assess the accuracy of its

508   response time-corrected data in the field. The sensor's slow response time likely limits the glider

509   to providing qualitative rather than quantitative results. However, due to the scarcity of oceanic

510   CH_4 observations, deploying a CH_4 glider can help identify the location of methane sources and

511   guide the placement of in situ observations to conduct a more quantitative assessment of CH_4

512   fluxes and dynamics.

513   Ocean gliders are part of the Intergovernmental Oceanographic Commission (IOC-

514   UNESCO) Global Ocean Observing System (GOOS) through the OceanGliders program

515   (https://www.oceangliders.org/). Like other elements of the GOOS coordinated by OceanOPs of

516   the Observation Coordination Group (floats, buoys, moorings, ships, and tide gauges),

517   OceanGliders contributes to "Ocean Observation for Climate, Ocean Health and Real Time

518   Services". CO_2 gliders are perfectly suited to contribute data for understanding relevant

519   inorganic carbon processes in coastal shelf and boundary regions where mesoscale or sub-

520   mesoscale variability dominates. The current work can also serve as a first step to bring together

521   interested scientists and engineers to further develop and improve the capability of gliders to

522   measure high-quality data. OceanGliders supports this effort by promoting the formation of

523   volunteer international task teams, for which a task team could be requested for oceanographic

524   greenhouse gas research. By doing this, the visibility and availability of data will be improved as

525   well, since GOOS provides an interactive data platform for all its programs (https://www.ocean-

526   ops.org/board). An OceanGliders task team could also be linked with the GOOS-sponsored

527   Global Climate Observing System (GCOS: https://gcos.wmo.int/en/home) program through their

528   Ocean Observations Physics and Climate Panel (OOPC): "a scientific expert advisory group

529   charged with making recommendations for a sustained global ocean observing system for

530   climate."

531

532   **5. Concluding Thoughts**

533   Near real-time and high-resolution water column data that can be retrieved from gliders

534   outfitted with sensors measuring salinity, temperature, inorganic carbon system parameters,

535   oxygen, and pCH$_4$ are key to tackling a variety of today's climate change-related issues. These

536   datasets will become instrumental in advancing biogeochemical model forecasting and early

537   warning systems for extreme heat, acidity, and oxygen compound events that affect coastal

538   subsistence communities, commercial fisheries, and mariculture. Furthermore, using

539   biogeochemical gliders to monitor the environment of tagged organisms (e.g. crabs, fish) would

540　provide insight into the organism's position and behavior relative to important environmental

541　drivers across susceptible ecosystems. Such biogeochemical glider data will help bridge in situ

542　chemical and biological measurements, and environmental change to impacts on biology, and

543　thereby fill an important research gap (Widdicomb et al., 2023). Potentially large natural and

544　anthropogenic sources of CH_4 may become contributors to climate change, and if oxidized, to

545　ocean acidification (Garcia-Tigreros et al., 2021; Sparrow et al., 2018; Shakhova et al., 2010;

546　Rees et al., 2022). These CH_4 sources need to be properly assessed and quantified, and if

547　characterized as anthropogenic origin, emitters must be held accountable (Goodman et al., 2022).

548　Once the combined HydroC CH_4/CO_2 is available it will provide a new tool to co-measure pCH_4

549　and pCO_2 and give valuable insight into these processes and feedback mechanisms. Other

550　advancing fields, such as marine Carbon Dioxide Removal (mCDR) and monitoring,

551　verification, and reporting (MRV) thereof will also need detailed knowledge of the distribution

552　of CO_2 in the water column (National Academies of Sciences, Engineering, and Medicine.

553　2022).

554　　　　The CO_2 Seaglider has been extensively tested and is ready to be used in open ocean

555　environments. An important next step will be to integrate the HydroC CO_2 and CH_4 sensors into

556　a glider platform that reliably functions in shallow, and freshwater-affected coastal areas, such as

557　the Gulf of Alaska, to be able to fill the large spatial and temporal data gap in these highly

558　dynamic areas.

559

560　**Data availability**

561　　　　The CO_2 Seaglider data is publicly available (Hauri et al., 2022; 2023). The HydroC-

562　specific SIRMA code and CNF file are available on Github (Cyprus-Subsea, 2024a and 2024b).

563   More detailed information on the HydroC – glider integration and operation can be found in the

564   CO_2 Seaglider Standard Operating Procedures (Irving et al., 2024).

565

566   **Author contributions**

567   C.H. and A.M. developed the research ideas and the proposal that funded this work. C.H.

568   led the fieldwork and writing of this manuscript. B.I. led the preparation for fieldwork and glider

569   data processing and analysis. D.H. led glider piloting for all trials. D.H. and E.A. assisted with

570   data processing, sensor programming, mechanical integration, glider ballasting, deployment, and

571   recovery. N.K. and J.K. provided technical support for the HydroC sensors. All authors

572   contributed to the writing of this manuscript.

573

574   **Competing interests**

575   Authors Hayes and Abdi are employed by AOOI and CSCS (respectively) and their

576   objective is to support the ocean research community by providing innovative, cutting-edge

577   observing technological solutions. These include autonomous platforms and related services in

578   unique configurations. Through the support of the National Science Foundation and the National

579   Oceanographic Partnership Program, AOOI was able to jointly develop the CO_2 and CH_4 gliders

580   and prove and improve the scientific utility of this approach. Authors Kinski and Kemme are

581   employed by -4H-JENA engineering GmbH, the manufacturer of the HydroC CO_2 and CH_4

582   sensors. The objective of -4H-JENA engineering GmbH is to provide best possible accuracy of

583   dissolved gas measurements on any platform and at any environmental condition. Intensive

584   collaboration with scientists is essential for the development of these products.

585

Acknowledgments

Financial support

References

610 **References**

611 Aßmann, S., Frank, C., and Körtzinger, A.: Spectrophotometric high-precision seawater pH

612 determination for use in underway measuring systems, Ocean Sci., 7, 597–607,

613 https://doi.org/10.5194/os-7-597-2011, 2011.

614

615 Barnes, R. O. and Goldberg, E. D. Methane production and consumption in anoxic marine

616 sediments. Geology 4, 297–300, 1976.

617

618 Bittig, H. C., Körtzinger, A., Neill, C., van Ooijen, E., Plant, J. N., Hahn, J., Johnson, K. S.,

619 Yang, B., and Emerson, S. R.: Oxygen Optode Sensors: Principle, Characterization, Calibration,

620 and Application in the Ocean, Front. Mar. Sci., 4, https://doi.org/10.3389/fmars.2017.00429,

621 2018.

622

623 Bockmon, E. E. and Dickson, A. G.: A seawater filtration method suitable for total dissolved

624 inorganic carbon and pH analyses, Limnology and Oceanography Methods, 12(4), 191–195,

625 https://doi.org/10.4319/lom.2014.12.191, 2014.

626

627 Breitberg, D., Salisbury, J., Bernhard, J., Cai, W.-J., Dupont, S., Doney, S., Kroeker, K., Levin,

628 L., Long, W. C., Milke, L., Miller, S., Phelan, B., Passow, U., Seibel, B., Todgham, A., and

629 Tarrant, A.: And on Top of All That… Coping with Ocean Acidification in the Midst of Many

630 Stressors, Oceanography, 25, 48–61, https://doi.org/10.5670/oceanog.2015.31, 2015.

631

632 Breitburg, D., Levin, L. A., Oschlies, A., Grégoire, M., Chavez, F. P., Conley, D. J., Garçon, V.,

633   Gilbert, D., Gutiérrez, D., Isensee, K., Jacinto, G. S., Limburg, K. E., Montes, I., Naqvi, S. W.

634   A., Pitcher, G. C., Rabalais, N. N., Roman, M. R., Rose, K. A., Seibel, B. A., Telszewski, M.,

635   Yasuhara, M., and Zhang, J.: Declining oxygen in the global ocean and coastal waters, Science,

636   359, 46, https://doi.org/10.1126/science.aam7240, 2018.

637

638   Briggs, E. M., Martz, T. R., Talley, L. D., Mazloff, M. R., and Johnson, K. S.: Physical and

639   Biological Drivers of Biogeochemical Tracers Within the Seasonal Sea Ice Zone of the Southern

640   Ocean From Profiling Floats, J. Geophys. Res. Oceans, 123, 746–758,

641   https://doi.org/10.1002/2017JC012846, 2018.

642

643   Chavez, F. P., Sevadjian, J., Wahl, C., Friederich, J., and Friederich, G. E.: Measurements of

644   pCO$_2$ and pH from an autonomous surface vehicle in a coastal upwelling system, Deep Sea Res.

645   Part II Top. Stud. Oceanogr., 151, 137–146, https://doi.org/10.1016/j.dsr2.2017.01.001, 2018.

646

647   Claustre, H., Johnson, K. S., and Takeshita, Y.: Observing the Global Ocean with

648   Biogeochemical-Argo, Annu. Rev. Mar. Sci., 12, 23–48, https://doi.org/10.1146/annurev-

649   marine-010419-010956, 2020.

650

651   Clayton, T. D. and Byrne, R. H.: Spectrophotometric seawater pH measurements: total hydrogen

652   ion concentration scale calibration of m-cresol purple and at-sea results, Deep Sea Res. Part

653   Oceanogr. Res. Pap., 40(10), 2115–2129, 1993.

654

655   Cyprus-Subsea: Smart-Cable-HydroC, GitHub repository [code], https://github.com/Cyprus-

656 Subsea/Smart-Cable-HydroC (last access: 14 June 2024), 2024a.

657

658 Cyprus-Subsea: CO_2 and CH_4 CNF files, GitHub repository [code], https://github.com/Cyprus-

659 Subsea/Smart-Cable-HydroC/tree/main/docs (last access: 7 July 2024), 2024b.

660

661 DeGrandpre, M. D., Lai, C. Z., Timmermans, M. L., Krishfield, R. A., Proshutinsky, A., and

662 Torres, D.: Inorganic Carbon and pCO_2 Variability During Ice Formation in the Beaufort Gyre of

663 the Canada Basin, J. Geophys. Res. Oceans, 124, 4017–4028,

664 https://doi.org/10.1029/2019JC015109, 2019.

665

666 Dickson, A. G.: Thermodynamics of the dissociation of boric acid in synthetic seawater from

667 273.15 to 318.15 K, Deep Sea Res. Part Oceanogr. Res. Pap., 37, 755–766,

668 https://doi.org/10.1016/0198-0149(90)90004-F, 1990.

669

670 Dickson, A. G. G., Sabine, C. L., Christian J.R., Christian, J. R., and Christian J.R.: Guide to

671 Best Practices for Ocean CO_2 Measurements, PICES Spec. Publ. 3, 191, 2007.

672

673 Dølven, K. O., Vierinen, J., Grilli, R., Triest, J., and Ferré, B.: Response time correction of slow-

674 response sensor data by deconvolution of the growth-law equation, Geosci. Instrum. Methods

675 Data Syst., 11, 293–306, https://doi.org/10.5194/gi-11-293-2022, 2022.

676

677 Doney, S. C., Fabry, V. J., Feely, R. A., and Kleypas, J. A.: Ocean Acidification: The Other CO_2

678 Problem, Annu. Rev. Mar. Sci., 1, 169–192,

679   https://doi.org/10.1146/annurev.marine.010908.163834, 2009.

680

681   Du, M. et al. High resolution measurements of methane and carbon dioxide in surface waters

682   over a natural seep reveal dynamics of dissolved phase air–sea flux. Environ. Sci. Technol. 48,

683   10165–10173 (2014).

684

685   Fiedler, B., Fietzek, P., Vieira, N., Silva, P., Bittig, H. C., and Körtzinger, A.: In situ CO_2 and O_2

686   measurements on a profiling float, J. Atmospheric Ocean. Technol., 30, 112–126,

687   https://doi.org/10.1175/JTECH-D-12-00043.1, 2013.

688

689   Fietzek, P., Fiedler, B., Steinhoff, T., and Körtzinger, A.: In situ quality assessment of a novel

690   underwater $p$$CO_2$ sensor based on membrane equilibration and NDIR spectrometry, J.

691   Atmospheric Ocean. Technol., 31, 181–196, https://doi.org/10.1175/JTECH-D-13-00083.1,

692   2014.

693

694   Garcia-Tigreros, F., Leonte, M., Ruppel, C. D., Ruiz-Angulo, A., Joung, D. J., Young, B., and

695   Kessler, J. D.: Estimating the Impact of Seep Methane Oxidation on Ocean pH and Dissolved

696   Inorganic Radiocarbon Along the U.S. Mid-Atlantic Bight, J. Geophys. Res. Biogeosciences,

697   126, e2019JG005621, https://doi.org/10.1029/2019JG005621, 2021.

698

699   Goodman, S., Davies, P., Maddox, M., and Durkee, J.: Arctic Methane – Situational Awareness,

700   Assessment and Policy Directions, Results of the June 23rd, 2022 Arctic Methane Workshop,

701   Summary Report, 2022.

702

703 Gruber, N., Clement, D., Carter, B. R., Feely, R. A., van Heuven, S., Hoppema, M., Ishii, M.,

704 Key, R. M., Kozyr, A., Lauvset, S. K., Lo Monaco, C., Mathis, J. T., Murata, A., Olsen, A.,

705 Perez, F. F., Sabine, C. L., Tanhua, T., and Wanninkhof, R.: The oceanic sink for anthropogenic

706 CO2 from 1994 to 2007, Science, 363, 1193–1199, https://doi.org/10.1126/science.aau5153,

707 2019.

708

709 Gruber, N., Boyd, P. W., Frölicher, T. L., and Vogt, M.: Biogeochemical extremes and

710 compound events in the ocean, Nature, 600, 395–407, https://doi.org/10.1038/s41586-021-

711 03981-7, 2021.

712

713 Hauri, C., McDonnell, A., Winsor, P., Irving, B., and Statscewich, H.: Development of an

714 Autonomous Carbon Glider to Monitor Sea-Air CO_2 Fluxes in the Chukchi Sea, Bureau of

715 Ocean Energy Management, 2018.

716

717 Hauri, C., Irving, B., Hayes, D., Abdi, E., Kemme, J., Kinski, N., McDonnell, A.M.P.: CO_2

718 Seaglider trajectory file from Gulf of Alaska 2022. SEANOE. https://doi.org/10.17882/100964,

719 2022.

720

721 Hauri, C., Irving, B., Hayes, D., Abdi, E., Kemme, J., Kinski, N., McDonnell, A.M.P.: CO_2

722 Seaglider trajectory file from Gulf of Alaska 2023. SEANOE. https://doi.org/10.17882/100965,

723 2023.

724

725   Hauri, C., Pagès, R., Hedstrom, K., Doney, S. C., Dupont, S., Ferriss, B., and Stuecker, M. F.:

726   More Than Marine Heatwaves: A New Regime of Heat, Acidity, and Low Oxygen Compound

727   Extreme Events in the Gulf of Alaska, AGU Adv., 5, e2023AV001039,

728   https://doi.org/10.1029/2023AV001039, 2024.

729

730   Hemming, M. P., Kaiser, J., Heywood, K. J., Bakker, D. C. E., Boutin, J., Shitashima, K., Lee,

731   G., Legge, O., and Onken, R.: Measuring pH variability using an experimental sensor on an

732   underwater glider, Ocean Sci., 13, 427–442, https://doi.org/10.5194/os-13-427-2017, 2017.

733

734   Irving, B., Hauri, C., Hayes, D., Abdi, E., Kinski., N.: Carbon Dioxide SOP, Version 1.0.0.

735   (GitHub Repository, Carbon Dioxide

736   SOP, https://britairving.github.io/Carbon_Dioxide_SOP/README.html (last access: 7 July,

737   2024).

738

739   Islam, F., DeGrandpre, M. D., Beatty, C. M., Timmermans, M.-L., Krishfield, R. A., Toole, J.

740   M., and Laney, S. R.: Sea surface CO_2 and O_2 dynamics in the partially ice-covered Arctic

741   Ocean, J. Geophys. Res. Oceans, 122, 1425–1438, https://doi.org/10.1002/2016JC012162, 2017.

742

743   Jiang, L.-Q., Feely, R. A., Wanninkhof, R., Greeley, D., Barbero, L., Alin, S., Carter, B. R.,

744   Pierrot, D., Featherstone, C., Hooper, J., Melrose, C., Monacci, N., Sharp, J. D., Shellito, S., Xu,

745   Y.-Y., Kozyr, A., Byrne, R. H., Cai, W.-J., Cross, J., Johnson, G. C., Hales, B., Langdon, C.,

746   Mathis, J., Salisbury, J., and Townsend, D. W.: Coastal Ocean Data Analysis Product in North

747   America (CODAP-NA) – an internally consistent data product for discrete inorganic carbon,

748   oxygen, and nutrients on the North American ocean margins, Earth Syst. Sci. Data, 13, 2777–

749   2799, https://doi.org/10.5194/essd-13-2777-2021, 2021.

750

751   Johnson, G. C. and Lyman, J. M.: Warming trends increasingly dominate global ocean, Nat.

752   Clim. Change, 10, 757–761, https://doi.org/10.1038/s41558-020-0822-0, 2020.

753

754   Kessler, J. Atlantic bubble bath. *Nature Geosci* **7**, 625–626, https://doi.org/10.1038/ngeo2238,

755   2014.

756

757   Kroeker, K. J., Kordas, R. L., and Harley, C. D. G.: Embracing interactions in ocean

758   acidification research: Confronting multiple stressor scenarios and context dependence, Biol.

759   Lett., 13, https://doi.org/10.1098/rsbl.2016.0802, 2017.

760

761   Laufkötter, C., Zscheischler, J., and Frölicher, T. L.: High-impact marine heatwaves attributable

762   to human-induced global warming, Science, 369, 1621–1625,

763   https://doi.org/10.1126/science.aba0690, 2020.

764

765   Lauvset, S. K., Lange, N., Tanhua, T., Bittig, H. C., Olsen, A., Kozyr, A., Alin, S., Álvarez, M.,

766   Azetsu-Scott, K., Barbero, L., Becker, S., Brown, P. J., Carter, B. R., da Cunha, L. C., Feely, R.

767   A., Hoppema, M., Humphreys, M. P., Ishii, M., Jeansson, E., Jiang, L.-Q., Jones, S. D., Lo

768   Monaco, C., Murata, A., Müller, J. D., Pérez, F. F., Pfeil, B., Schirnick, C., Steinfeldt, R.,

769   Suzuki, T., Tilbrook, B., Ulfsbo, A., Velo, A., Woosley, R. J., and Key, R. M.:

770   GLODAPv2.2022: the latest version of the global interior ocean biogeochemical data product,

771 Earth Syst. Sci. Data, 14, 5543–5572, https://doi.org/10.5194/essd-14-5543-2022, 2022.

772

773 Lee, K., Kim, T.-W., Byrne, R. H., Millero, F. J., Feely, R. A., and Liu, Y.-M.: The universal

774 ratio of boron to chlorinity for the North Pacific and North Atlantic oceans, Geochim.

775 Cosmochim. Acta, 74, 1801–1811, https://doi.org/10.1016/j.gca.2009.12.027, 2010.

776

777 Leonte, M., Kessler, J. D., Kellermann, M. Y., Arrington. E. C., Valentine, D. L., Sylva, S. P.

778 Rapid rates of aerobic methane oxidation at the feather edge of gas hydrate stability in the

779 waters of Hudson Canyon, US Atlantic Margin. Geochim. Cosmochim. Acta 204, 375–387,

780 https://doi.org/10.1016/j.gca.2017.01.009, 2017.

781

782 Lueker, T. J., Dickson, A. G., and Keeling, C. D.: Ocean pCO$_2$ calculated from dissolved

783 inorganic carbon , alkalinity , and equations for K 1 and K 2 : validation based on laboratory

784 measurements of CO$_2$ in gas and seawater at equilibrium, Mar. Chem., 70, 105–119,

785 https://doi.org/10.1016/S0304-4203(00)00022-0, 2000.

786

787 Manley, J. and Willcox, S.: The Wave Glider: A persistent platform for ocean science, in:

788 OCEANS'10 IEEE SYDNEY, OCEANS'10 IEEE SYDNEY, 1–5,

789 https://doi.org/10.1109/OCEANSSYD.2010.5603614, 2010.

790

791 McGinnis, D. F., Greinert, J., Artemov, Y., Beaubien, S. E. & Wüest, A. Fate of rising methane

792 bubbles in stratified waters: How much methane reaches the atmosphere? J. Geophys. Res. 111,

793 https://doi.org/10.1029/2005jc003183, 2006.

794

795   Metzl, N., Fin, J., Lo Monaco, C., Mignon, C., Alliouane, S., Antoine, D., Bourdin, G., Boutin,

796   J., Bozec, Y., Conan, P., Coppola, L., Diaz, F., Douville, E., Durrieu de Madron, X., Gattuso, J.-

797   P., Gazeau, F., Golbol, M., Lansard, B., Lefèvre, D., Lefèvre, N., Lombard, F., Louanchi, F.,

798   Merlivat, L., Olivier, L., Petrenko, A., Petton, S., Pujo-Pay, M., Rabouille, C., Reverdin, G.,

799   Ridame, C., Tribollet, A., Vellucci, V., Wagener, T., and Wimart-Rousseau, C.: A synthesis of

800   ocean total alkalinity and dissolved inorganic carbon measurements from 1993 to 2022: the

801   SNAPO-CO2-v1 dataset, Earth Syst. Sci. Data, 16, 89–120, https://doi.org/10.5194/essd-16-89-

802   2024, 2024.

803

804   Meurer, W. P., Blum, J., and Shipman, G.: Volumetric Mapping of Methane Concentrations at

805   the Bush Hill Hydrocarbon Seep, Gulf of Mexico, Front. Earth Sci., 9,

806   https://doi.org/10.3389/feart.2021.604930, 2021.

807

808   Monacci, N.M.; Bott, R.; Cross, J.N.; Dougherty, S.; Maenner, S.; Musielewicz, S.; Osborne, J.;

809   Sutton, A. (2023). High-resolution ocean and atmosphere $p\mathrm{CO_2}$ time-series measurements from

810   mooring GAKOA_149W_60N. High-resolution ocean and atmosphere $p\mathrm{CO_2}$ time-series

811   measurements from mooring GAKOA_149W_60N in the Gulf of Alaska (NCEI Accession

812   0116714). NOAA National Centers for Environmental Information. Dataset.

813   https://doi.org/10.3334/cdiac/otg.tsm_gakoa_149w_60n

814

815   Manley, J. and Willcox, S.: The Wave Glider: A persistent platform for ocean science, in:

816   OCEANS'10 IEEE SYDNEY, OCEANS'10 IEEE SYDNEY, 1–5,

817   https://doi.org/10.1109/OCEANSSYD.2010.5603614, 2010.

818

819   Miloshevich, L. M., Paukkunen, A., Vömel, H., and Oltmans, S. J.: Development and Validation

820   of a Time-Lag Correction for Vaisala Radiosonde Humidity Measurements, J. Atmospheric

821   Ocean. Technol., 21, 1305–1327, https://doi.org/10.1175/1520-

822   0426(2004)021<1305:DAVOAT>2.0.CO;2, 2004.

823

824   Myhre, G., Shindell, D., Bréon, F.-M., Collins, W., Fuglestvedt, J., Huang, J., Koch, D.,

825   Lamarque, J.-F., Lee, D., Mendoza, B., Nakajima, T., Robock, A., Stephens, G., Takemura, T.,

826   and Zhang, H.: Anthropogenic and Natural Radiative Forcing, in: Climate Change 2013: The

827   Physical Science Basis, Contribution of Working Group I to the Fifth Assessment Report of the

828   Intergovernmental Panel on Climate Change, edited by: Stocker, T. F., Qin, D., Plattner, G.-K.,

829   Tignor, M., Allen, S. K., Boschung, J., Nauels, A., Xia, Y., Bex, V., and Midgley, P. M.,

830   Cambridge University Press, Cambridge, UK, New York, NY, USA, 2013.

831

832   National Academies of Sciences, Engineering, and Medicine: A Research Strategy

833   for Ocean-based Carbon Dioxide Removal and Sequestration. Washington, DC: The National

834   Academies Press. https://doi.org/10.17226/26278, 2022.

835

836   Newton, J. A., Feely, R. A., Jewett, E. B., Williamson, P., and Mathis, J.: Global ocean

837   acidification observing network: requirements and governance plan, GOA-ON, Washington, 61

838   pp., 2015.

839

840   Nickford, S., Palter, J. B., Donohue, K., Fassbender, A. J., Gray, A. R., Long, J., Sutton, A. J.,

841   Bates, N. R., and Takeshita, Y.: Autonomous Wintertime Observations of Air-Sea Exchange in

842   the Gulf Stream Reveal a Perfect Storm for Ocean CO_2 Uptake, Geophys. Res. Lett., 49,

843   e2021GL096805, https://doi.org/10.1029/2021GL096805, 2022.

844

845   von Oppeln-Bronikowski, N., de Young, B., Atamanchuk, D., and Wallace, D.: Glider-based

846   observations of CO_2 in the Labrador Sea, Ocean Sci., 17, 1–16, https://doi.org/10.5194/os-17-1-

847   2021, 2021.

848

849   OceanGliders Oxygen SOP: https://nora.nerc.ac.uk/id/eprint/533559/, last access: 24 January

850   2024.

851

852   Orr, J. C., Epitalon, J. M., Dickson, A. G., and Gattuso, J. P.: Routine uncertainty propagation

853   for the marine carbon dioxide system, Mar. Chem., 207, 84–107,

854   https://doi.org/10.1016/j.marchem.2018.10.006, 2018.

855

856   Perez, F. F. and Fraga, F.: Association constant of fluoride and hydrogen ions in seawater, Mar.

857   Chem., 21, 161–168, https://doi.org/10.1016/0304-4203(87)90036-3, 1987.

858

859   Pinnau, I., and Toy, L. G.: Gas and vapor transport properties of amorphous perfluorinated

860   copolymer membranes based on 2,2-bistrifluoromethyl-4,5-difluoro-1,3-

861   dioxole/tetrafluoroethylene, Journal of Membrane Science, 109 (1), 125-133,

862   https://doi.org/10.1016/0376-7388(95)00193-X, 1996.

863

864   Possenti, L., Humphreys, M. P., Bakker, D. C. E., Cobas-García, M., Fernand, L., Lee, G. A.,

865   Pallottino, F., Loucaides, S., Mowlem, M. C., and Kaiser, J.: Air-Sea Gas Fluxes and

866   Remineralization From a Novel Combination of pH and O_2 Sensors on a Glider, Front. Mar. Sci.,

867   8, 1–19, https://doi.org/10.3389/fmars.2021.696772, 2021.

868

869   Reeburgh, W. Oceanic methane biogeochemistry. Am. Chem. Soc. 107, 486–513, 2007.

870

871   Sarmiento, J. L. and Gruber, N.: Ocean Biogeochemical Dynamics, Princeton University Press,

872   Princeton, NJ, 526 pp., ISBN 9780691017075, 2006.

873

874   Qi, D., Ouyang, Z., Chen, L., Wu, Y., Lei, R., Chen, B., Feely, R. A., Anderson, L. G., Zhong,

875   W., Lin, H., Polukhin, A., Zhang, Y., Zhang, Y., Bi, H., Lin, X., Luo, Y., Zhuang, Y., He, J.,

876   Chen, J., and Cai, W. J.: Climate change drives rapid decadal acidification in the Arctic Ocean

877   from 1994 to 2020, Science, 377, 1544–1550, https://doi.org/10.1126/science.abo0383, 2022.

878

879   Rees, A. P., Bange, H. W., Arévalo-Martínez, D. L., Artioli, Y., Ashby, D. M., Brown, I.,

880   Campen, H. I., Clark, D. R., Kitidis, V., Lessin, G., Tarran, G. A., and Turley, C.: Nitrous oxide

881   and methane in a changing Arctic Ocean, Ambio, 51, 398–410, https://doi.org/10.1007/s13280-

882   021-01633-8, 2022.

883

884   Saba, G. K., Wright-Fairbanks, E., Chen, B., Cai, W. J., Barnard, A. H., Jones, C. P., Branham,

885   C. W., Wang, K., and Miles, T.: The Development and Validation of a Profiling Glider Deep

886   ISFET-Based pH Sensor for High Resolution Observations of Coastal and Ocean Acidification,

887   Front. Mar. Sci., 6, 1–17, https://doi.org/10.3389/fmars.2019.00664, 2019.

888

889   Sabine, C. L. and Tanhua, T.: Estimation of anthropogenic CO_2 inventories in the ocean., Annu.

890   Rev. Mar. Sci., 2, 175–98, https://doi.org/10.1146/annurev-marine-120308-080947, 2010.

891

892   Sabine, C. L., Feely, R. A., Gruber, N., Key, R. M., Lee, K., Bullister, J. L., Wanninkhof, R.,

893   Wong, C. S., Wallace, D. W. R., Tilbrook, B., Millero, F. J., Peng, T.-H., Kozyr, A., Ono, T.,

894   and Rios, A. F.: The oceanic sink for anthropogenic CO_2, Science, 305, 367–71,

895   https://doi.org/10.1126/science.1097403, 2004.

896

897   Sejr, M. K., Krause-Jensen, D., Rysgaard, S., Sørensen, L. L., Christensen, P. B., and Glud, R.

898   N.: Air-sea flux of CO_2 in arctic coastal waters influenced by glacial melt water and sea ice,

899   Tellus B, 63, 815–822, https://doi.org/10.1111/j.1600-0889.2011.00540.x, 2011.

900

901   Sharp, J. D., Pierrot, D., Humphreys, M. P., Epitalon, J.-M., Orr, J. C., Lewis, E. R., and

902   Wallace, D. W. R.: CO2SYSv3 for MATLAB, , https://doi.org/10.5281/zenodo.7552554, 2023.

903

904   Shakhova, N., Semiletov, I., Salyuk, A., Yusupov, V., Kosmach, D., and Gustafsson, Ö.:

905   Extensive Methane Venting to the Atmosphere from Sediments of the East Siberian Arctic Shelf,

906   Science, 327, 1246–1250, https://doi.org/10.1126/science.1182221, 2010.

907

Skarke, A., Ruppel, C., Kodis, M., Brothers, D. and Lobecker, E. Widespread methane leakage

from the sea floor on the northern US Atlantic margin. Nat. Geosci. 7, 657 (2014).

910

Sparrow, K. J., Kessler, J. D., Southon, J. R., Garcia-Tigreros, F., Schreiner, K. M., Ruppel, C.

D., Miller, J. B., Lehman, S. J., and Xu, X.: Limited contribution of ancient methane to surface

waters of the U.S. Beaufort Sea shelf, Sci. Adv., 4, eaao4842,

https://doi.org/10.1126/sciadv.aao4842, 2018.

915

Sulpis, O., Lauvset, S. K., and Hagens, M.: Current estimates of K and K appear inconsistent

with measured CO_2 system parameters in cold oceanic regions, Ocean Sci., 16, 847–

862, https://doi.org/10.5194/os-16-847-2020, 2020.

919

Takeshita, Y., Jones, B. D., Johnson, K. S., Chavez, F. P., Rudnick, D. L., Blum, M., Conner, K.,

Jensen, S., Long, J. S., Maughan, T., Mertz, K. L., Sherman, J. T., and Warren, J. K.: Accurate

pH and O_2 Measurements from Spray Underwater Gliders, J. Atmospheric Ocean. Technol., 38,

181–195, https://doi.org/10.1175/JTECH-D-20-0095.1, 2021.

924

Thompson, T., Saba, G. K., Wright-Fairbanks, E., Barnard, A. H., and Branham, C. W.: Best

Practices for Sea-Bird Scientific deep ISFET-based pH sensor integrated into a Slocum Webb

Glider, in: OCEANS 2021: San Diego – Porto, OCEANS 2021: San Diego – Porto, 1–8,

https://doi.org/10.23919/OCEANS44145.2021.9706067, 2021.

929

930   Vergara-Jara, M. J., DeGrandpre, M. D., Torres, R., Beatty, C. M., Cuevas, L. A., Alarcón, E.,

931   and Iriarte, J. L.: Seasonal changes in carbonate saturation state and air-sea CO_2 fluxes during an

932   annual cycle in a stratified-temperate fjord (Reloncaví Fjord, Chilean Patagonia), J. Geophys.

933   Res. Biogeosciences, 124, 2851–2865, https://doi.org/10.1029/2019jg005028, 2019.

934

935   Widdicombe, S., Isensee, K., Artioli, Y., Gaitán-Espitia, J. D., Hauri, C., Newton, J. A.,

936   et al.: Unifying biological field observations to detect and compare ocean acidification impacts

937   across marine species and ecosystems: What to monitor and why. *Ocean Science*, **19**(1), 101–

938   119. https://doi.org/10.5194/os-19-101-2023, 2023.

939

940   Woosley, R. J. and Millero, F. J.: Freshening of the western Arctic negates anthropogenic carbon

941   uptake potential, Limnol. Oceanogr., https://doi.org/10.1002/lno.11421, 2020.

942

943   Wright-Fairbanks, E. K., Miles, T. N., Cai, W.-J., Chen, B., and Saba, G. K.: Autonomous

944   Observation of Seasonal Carbonate Chemistry Dynamics in the Mid-Atlantic Bight, J. Geophys.

945   Res. Oceans, 125, e2020JC016505, https://doi.org/10.1029/2020JC016505, 2020.

946
947

948

949

950

951 **Tables**

952 **Table 1. Tank experiment.** Evaluation of SG HydroC CO_2 and SG HydroC CH_4 sensors

953 compared to reference discrete pCO_2^{disc} and pCH_4^{disc}. Units of pCO_2 and $pCH4$ are µatm except

954 when shown as percent difference in parenthesis (Equation 1). Columns with subscripts sn422

955 and sn0718 indicate data from sensors HydroC CO2T-0422-001 and HydroC CO2T-0718-001,

956 respectively. Superscript RTC indicates response time corrected values following Dølven et al.

957 (2022). pCO_2^{disc} and pCH_4^{disc} values are the average of triplicate bottles and are shown in Figure

958 4.

959

Triplicate Date Time (UTC)	$pCO_2^{disc} \pm$ uc (µatm)	$pCO_{2,sn422}^{RTC}$ - pCO_2^{disc}	$pCO_{2,sn0718}^{RTC}$ - pCO_2^{disc}	$pCH_4^{disc} \pm$ u (µatm)	pCH_4^{RTC} - pCH_4^{disc}
5/2/2022 3:25	298.7 ± 10.2	-0.9 (0.3 %)	-	-	-
5/2/2022 7:32	227.1 ± 7.8	4.3 (1.9 %)	2.4 (1.1 %)	-	-
5/2/2022 11:27	223.3 ± 7.7	0.7 (0.3 %)	-2.6 (1.2 %)	-	-
5/2/2022 15:30	227.8 ± 7.9	-1.1 (0.5 %)	-3.3 (1.5 %)	-	-
5/2/2022 00:11	-	-	-	25.4 ± 2.1	4.0 (14.6 %)
5/2/2022 12:06	-	-	-	7.3 ± 1.3	0.5 (6.3 %)

960

961

962   **Table 2. Profiling experiment.** Evaluation of SG HydroC CO_2 sensor compared to reference

963   discrete pCO_2^{disc}. Units of pCO_2 are µatm except when shown as percent difference in

964   parenthesis (Eq. 1). pCO_2 with subscripts sn422 indicate data from the HydroC installed on the

965   rosette (HydroC CO2T-0422-001). The superscript RTC indicates response time corrected values

966   following Dølven et al. (2022).

Discrete Date Time (UTC)	Discrete Depth (m)	$pCO_2^{disc} \pm$ uc (µatm)	$pCO_{2,sn422}^{RTC} - pCO_2^{disc}$
5/3/2022 21:21	2.5	214.5 ± 7.5	5.4 (2.5%)
5/3/2022 21:39	19.9	246.8 ± 8.5	1.6 (0.6 %)
5/3/2022 22:33	9.6	244.4 ± 8.5	-3.3 (1.4 %)
5/3/2022 22:34	9.7	234.7 ± 8.1	8.2 (3.4 %)

967

968

969 **Table 3. Seaglider HydroC evaluation with a nearby cast.** Evaluation of Seaglider integrated

970 and rosette mounted SG HydroC CO2 sensors compared to pCO_2^{disc} collected from a nearby cast.

971 Units of pCO_2 are µatm except when shown as percent difference in parenthesis (Eq. 1) and

972 differences between $pCO_{2,Seaglider}^{RTC}$ were calculated with the average (upcast and downcast

973 combined) 1-meter binned data. The superscript RTC indicates response time corrected values

974 following Dølven et al. (2022), and subscripts Rosette and Seaglider indicate the SG HydroC

975 CO_2 sensor mounted on the rosette (SG HydroC CO2T-0422-001) and integrated into the

976 Seaglider (SG HydroC CO2T-0718-001), respectively. Time delay (HH:MM) and spatial

977 distance (km) columns represent the distance between $pCO_{2,Seaglider}^{RTC}$ measured at the discrete

978 depth and the discrete date time. The asterisk (*) indicates the comparison with $pCO_{2,Rosette}^{RTC}$

979 taken as nearest in time before sensor zeroing (Figure S1).

Discrete Date Time (UTC)	Discrete Depth (m)	$pCO_2^{disc} \pm uc$ (µatm)	$pCO_{2,Rosette}^{RTC}$ - pCO_2^{disc}	Delay (HH:MM)	Distance (km)	$pCO_{2,Seaglider}^{RTC}$ - pCO_2^{disc}
5/7/2022 18:06	71.8	349.7 ± 7.8	-5.7 (1.6 %)	02:47	0.4	10.2 (2.9 %)
5/7/2022 18:24	57.1	313.8 ± 6.7	12.1 (3.8 %)	03:05	0.6	8.3 (2.6 %)
5/7/2022 18:42	19.8	285.3 ± 6.1	0.8 (0.3 %)	03:23	0.8	8.6 (3.0 %)
5/7/2022 19:00	1.6	233.4 ± 5.0	-2.3 (1.0 %)*	03:41	0.9	12.0 (5.0 %)

980

981
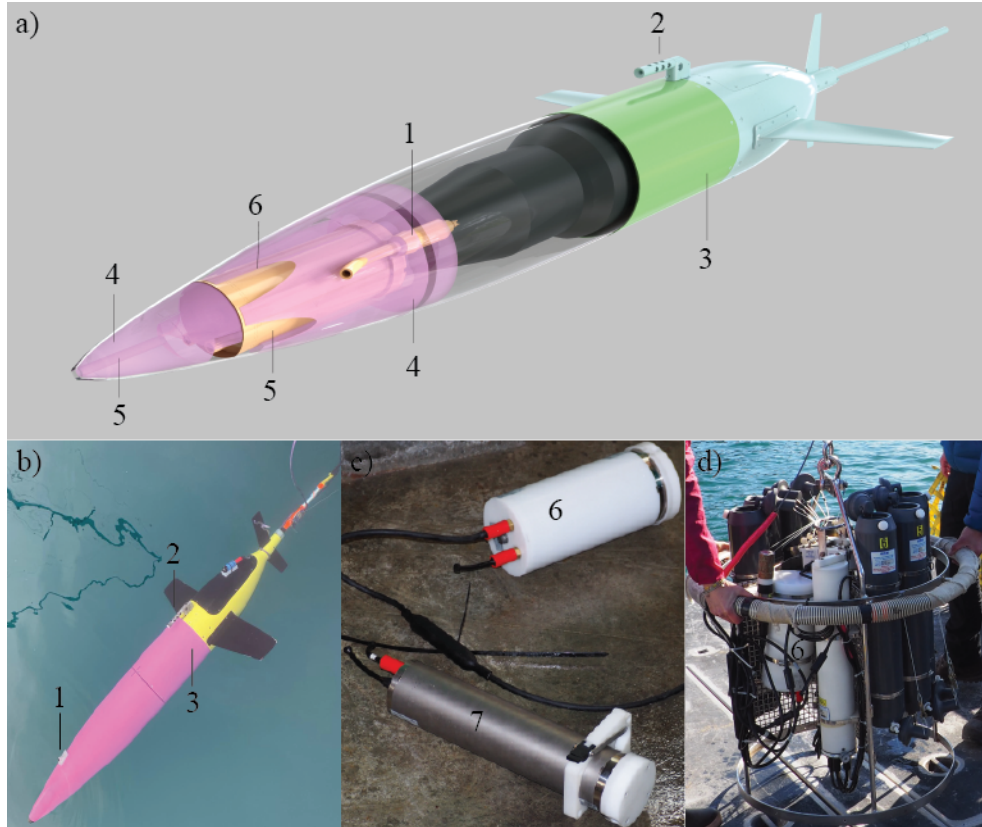
Figures

983

984 **Figure 1. CO$_2$ Seaglider.** CO$_2$ Seaglider a) schematic rendering and b) picture in Resurrection

985 Bay, Seward, Alaska, during a checkout dive on 6 February, 2023, before beginning the first

986 winter mission collecting high resolution pCO$_2$ data. Highlighted are 1) SeaBird 5M pump, 2)

987 conductivity and temperature sail, 3) extension, 4) syntactic foam, 5) water flow channels, and 6)

988 SG HydroC CO$_2$ in a titanium housing, enabling pCO$_2$ observations down to 1000 m. c) Picture

989 of new SG HydroC CO$_2$ in a POM housing (6, rated to 300 m depth) and original CONTROS

990 HydroC^{TM} CO$_2$ (7). d) Picture of rosette set up for profiling experiment.

991

Figure 2. SG HydroC CO$_2$ sensor mounting designs. a) Titanium SG HydroC CO$_2$ (rated to

1000m) in a custom syntactic foam coat and b) POM SG HydroC CO$_2$ (rated to 300m) with

brackets.
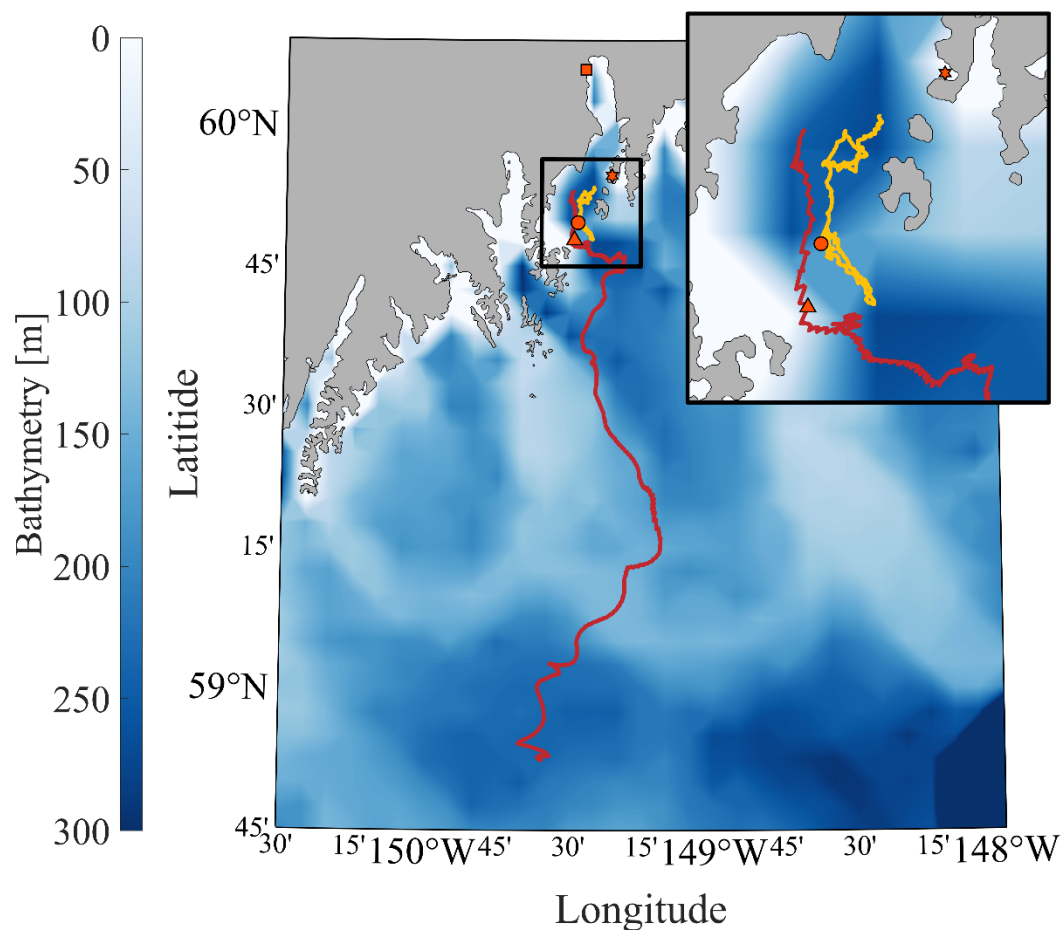
Figure 3. Map of CO₂ Seaglider study area. The bathymetry of the Gulf of Alaska is shown in color with zoomed in section of the head of Resurrection Bay (outlined black square and inset map). Tracks of the CO₂ Seaglider from the May 2022 and February 2023 missions are shown in yellow and red, respectively. Orange markers outlined in black show the location of the Alutiiq Pride Marine Institute (square), National Oceanic and Atmospheric Administration's Gulf of Alaska Ocean Acidification mooring (star), May 7th CTD cast (circle), and last location where pCO₂ was collected during the February 2023 mission (triangle).

1004
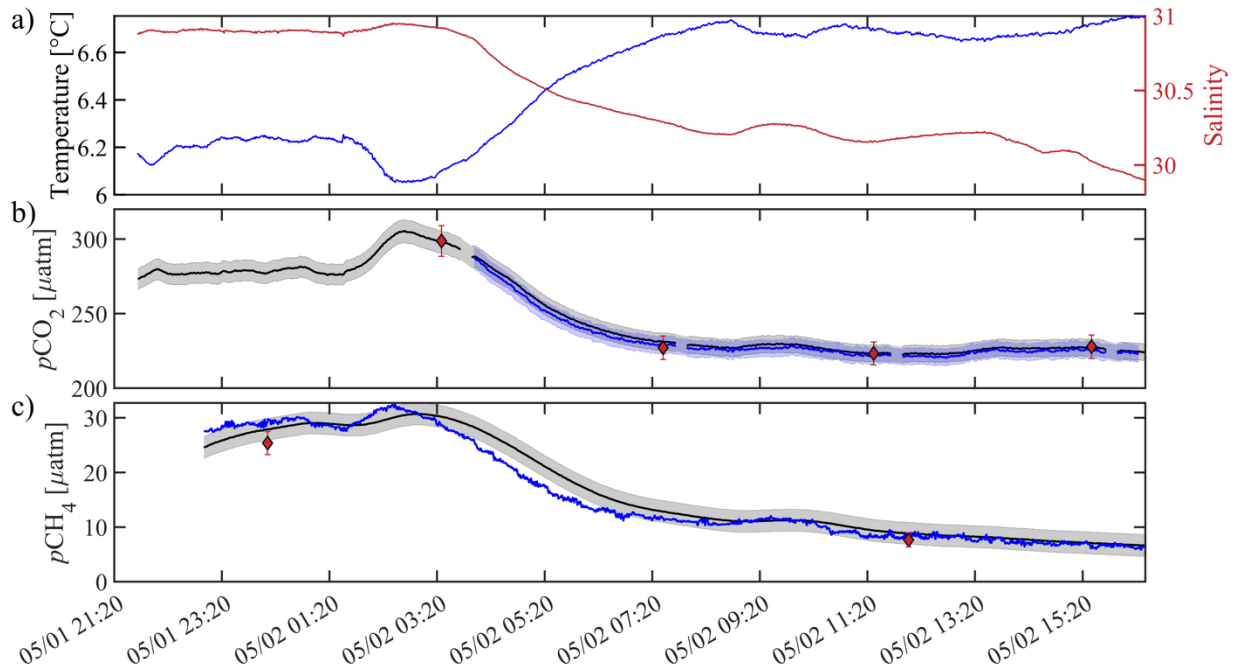
Figure 4. Sensor validation during a tank experiment at the Alutiiq Pride Marine Institute on May 1 – 2, 2022. a) temperature (blue line) and salinity (red line) from a recently calibrated Sea-Bird Scientific SBE37. b) black (blue) lines show pCO_2 in µatm from HydroC CO2T-0422-001 (HydroC CO2T-0718-001) with the shaded gray (blue) areas showing a relative uncertainty of 2.5% (weather quality goal; Newton et al., 2015). Black circles with red filling show discrete pCO_2^{disc} with error bars showing the combined standard uncertainty from *errors.m* (Orr et al., 2018). HydroC pCO_2 data are shown at 1 minute resolution with a 2-minute moving median filter applied and have not been corrected for response time, but differences were negligible (< 0.1 µatm). c) Black line shows pCH_4 in µatm from HydroC CH4T-0422-001 with the shaded gray bar showing an uncertainty of 2 µatm. The blue line is the response time corrected signal with a response time of 43 minutes following Dølven et al., (2022). HydroC pCH_4 data are shown at 1 minute resolution with a 2-minute moving median filter applied to the raw data and a

50

1017   10-minute moving median filter applied to the RTC data. Black diamonds with red filling show

1018   discrete $p\mathrm{CH_4}^{\mathrm{disc}}$ and all discrete values of $p\mathrm{CO_2}^{\mathrm{disc}}$ and $p\mathrm{CH_4}^{\mathrm{disc}}$ are the average of triplicate

1019   bottles.

1020

1021
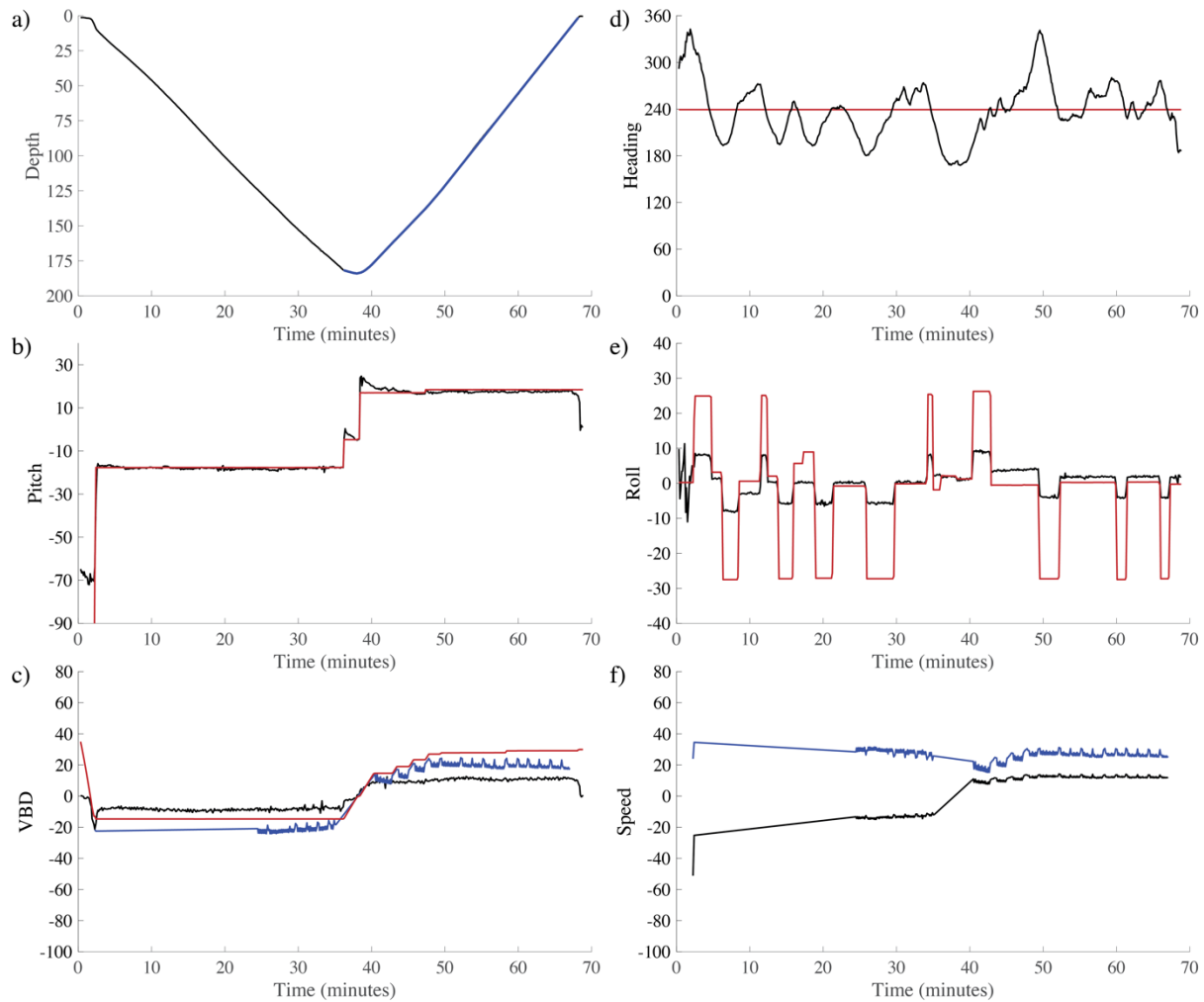
1022

1023 **Figure 5. Dive details for the 300 m rated CO₂ Seaglider (dive# 51).** a) Depth (black line,

1024 meters), b) pitch (black line, degrees) with pitch control (red line, mm of battery shift), c)

1025 Change in displacement of Variable Buoyancy Drive (VBD) (red line, units of 10 cc), vertical

1026 velocity from pressure measurements (black line, cm/s), and buoyancy (blue line, units of 10 g),

1027 d) heading in (desired red line, measured black line, degrees), e) roll (battery roll position red

1028 line, glider measured roll black line, degrees), and f) vertical speed (calculated from buoyancy

1029 and pitch, black line, cm/s) and horizontal speed (calculated from buoyancy and pitch, blue line,

1030 cm/s).

52
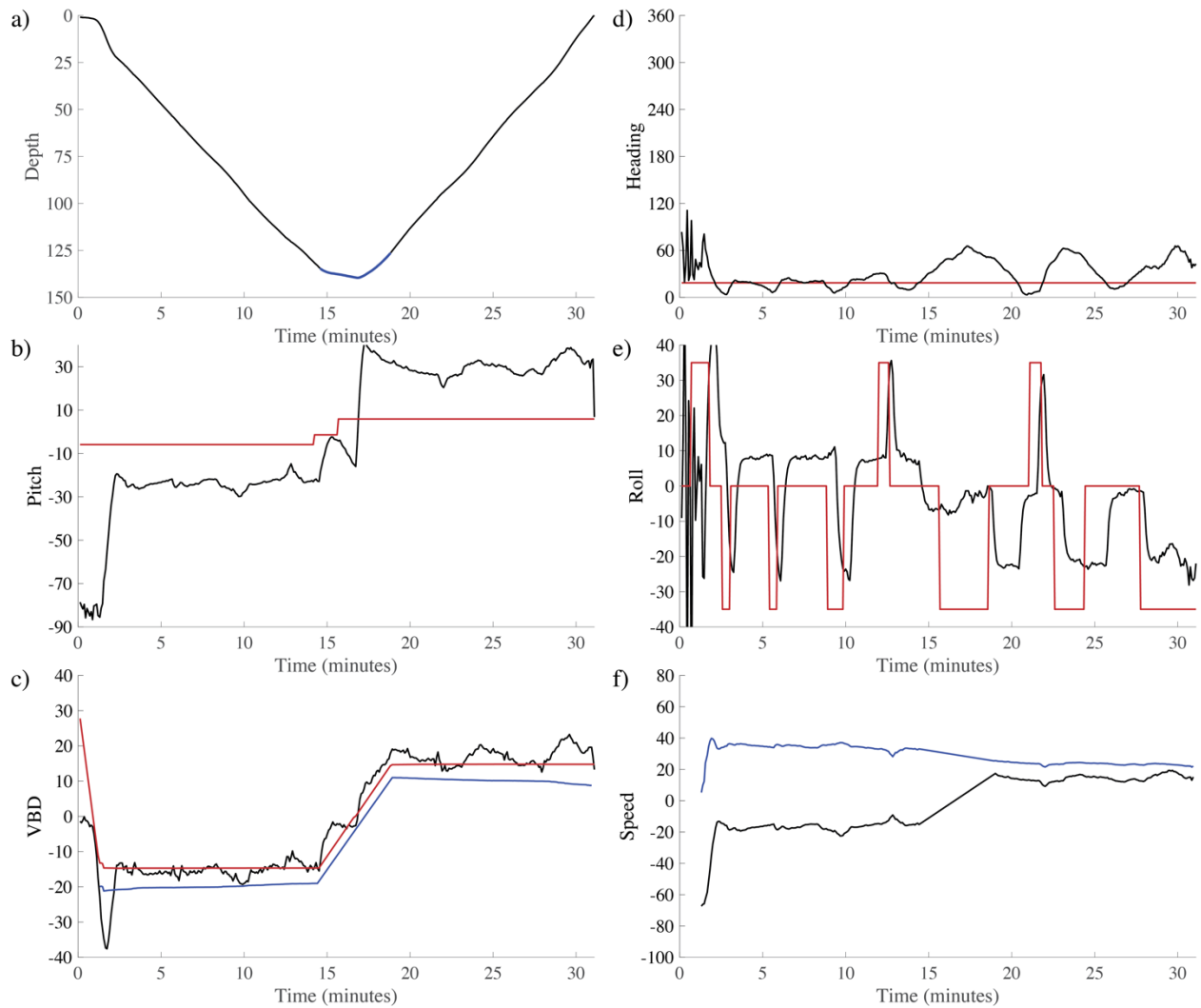
1031

Figure 6. Dive details for the 1000 m rated CO₂ Seaglider (dive# 203). a) Depth (black line,

meters), b) pitch (black line, degrees) with pitch control (red line, mm of battery shift), c)

Change in displacement of Variable Buoyancy Drive (VBD) (red line, units of 10 cc), vertical

velocity from pressure measurements (black line, cm/s), and buoyancy (blue line, units of 10 g),

d) Heading (desired heading red line, measured heading black line, degrees) e) roll (battery roll

position red line, glider measured roll black line, degrees), and f) vertical speed (calculated from

buoyancy and pitch, black line, cm/s) and horizontal speed in cm/s (calculated from buoyancy

and pitch, blue line, cm/s).

53
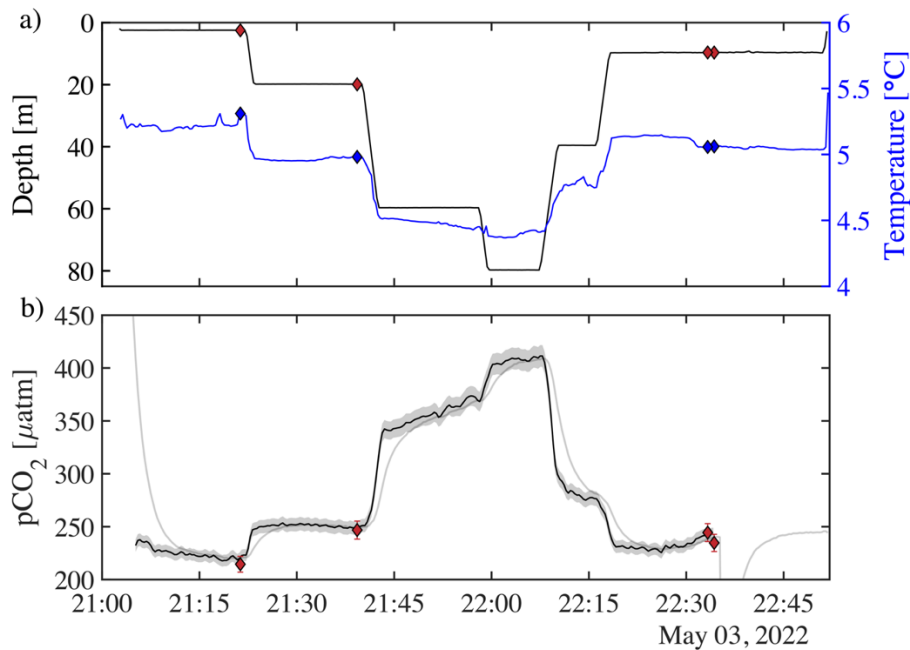
1040

Figure 7. Profiling experiments from May 3rd with HydroC CO2T-0422-001 sensor

mounted on the rosette. a) Pressure vs time on the left (black) axis with diamonds showing

rosette CTD values of pressure (red filled diamond), and temperature vs time on the right (blue)

axis and temperature (blue filled diamond) at the time of the bottle fire. b) pCO_2 measured by

the rosette mounted SG HydroC CO_2 sensor as raw (gray line) and response time corrected

signal (thick black line; $pCO_{2,sn422}^{RTC}$ in Table 2) with shaded relative uncertainty of 2.5%

(weather goal; Newton et al., 2015). pCO_2^{disc} shown as red diamonds with vertical red error bars

showing combined standard uncertainty (Orr et al., 2018). Table 2 shows differences between

discrete pCO_2^{disc} and $pCO_{2,sn422}^{RTC}$. The SG HydroC CO_2 sensor started a zeroing interval at

22:35 on May 3, 2022, so $pCO_{2,sn422}^{RTC}$ is not shown after that time but signal recovery can be

seen in the uncorrected signal (gray line).

1052

1053
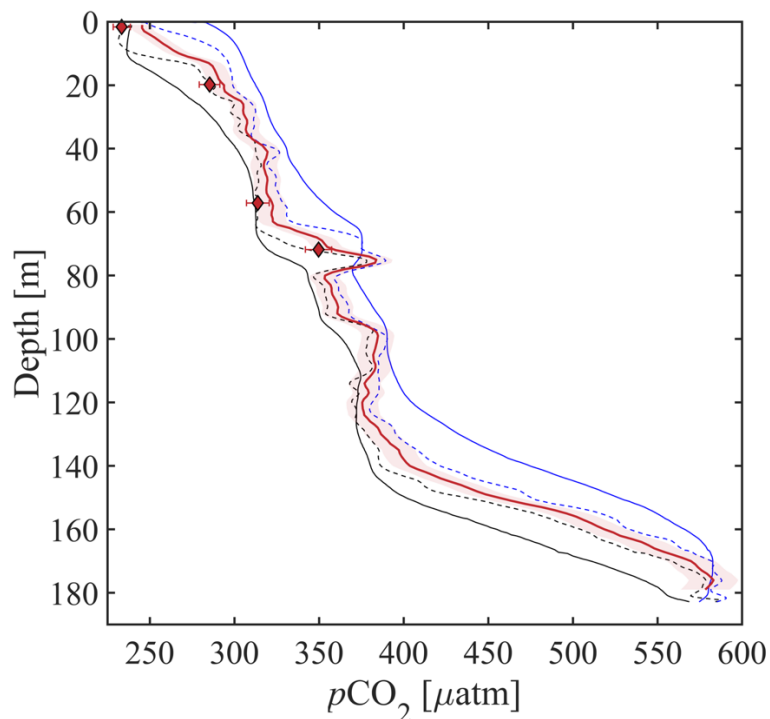

1054

1055 **Figure 8. CO₂ Seaglider data from a sea trial mission in May 2022 in Resurrection Bay,**

1056 **Seward, Alaska.** Depth profile of pCO_2 in µatm showing the original resolution smoothed pCO_2

1057 used in the RT correction (downcast = solid black, upcast = solid blue), RTC pCO_2 following

1058 Dølven et al. (2022) (dashed black line = downcast, dashed blue line = upcast), and 1-meter

1059 binned RTC profile (thick red line) with red shading showing the relative uncertainty of 2.5 %.

1060 Discrete pCO_2^{disc} shown as red diamonds with horizontal red error bars showing combined

1061 standard uncertainty (Orr et al., 2018). Differences between pCO_2^{disc} and $pCO_{2,Seaglider}^{RTC}$ are

1062 shown in Table 3.

1063
1064
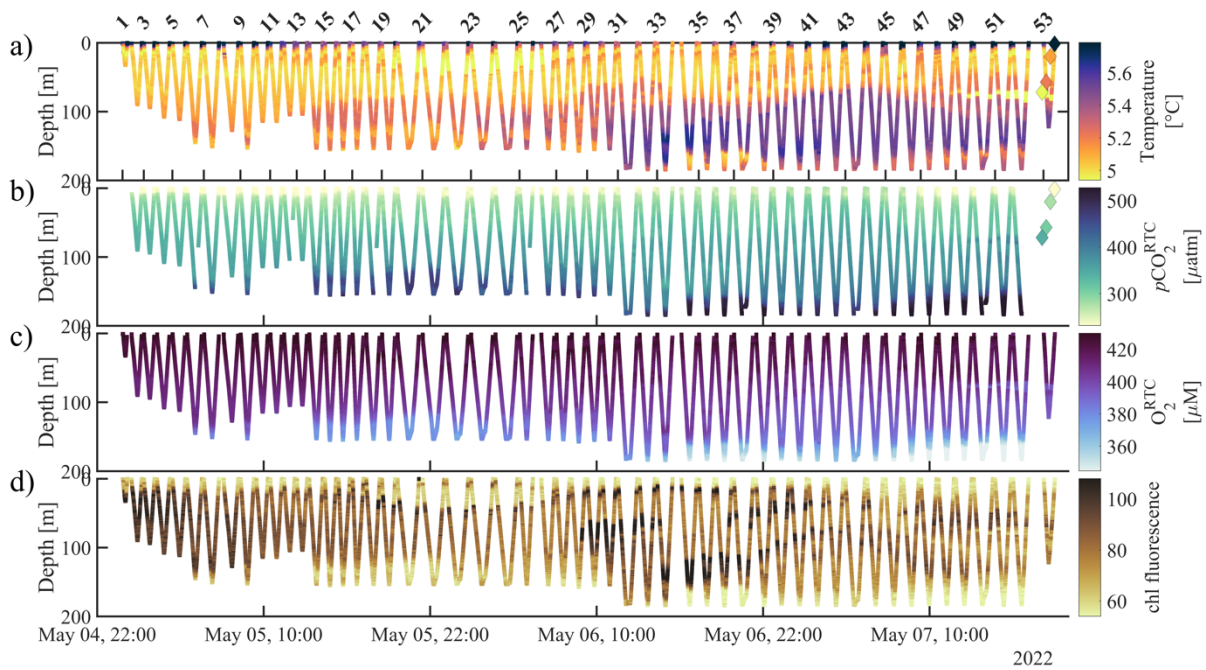
1065

Figure 9. CO₂ Seaglider data from a sea trial mission in spring 2022 in Resurrection Bay, Seward, Alaska. Depth profiles of a) Temperature [°C], b) RTC pCO$_2$ [µatm] c) RTC O$_2$ [µM], and d) raw chlorophyll fluorescence. The diamonds show discrete values that were taken during a CTD cast (Table 3).

1070
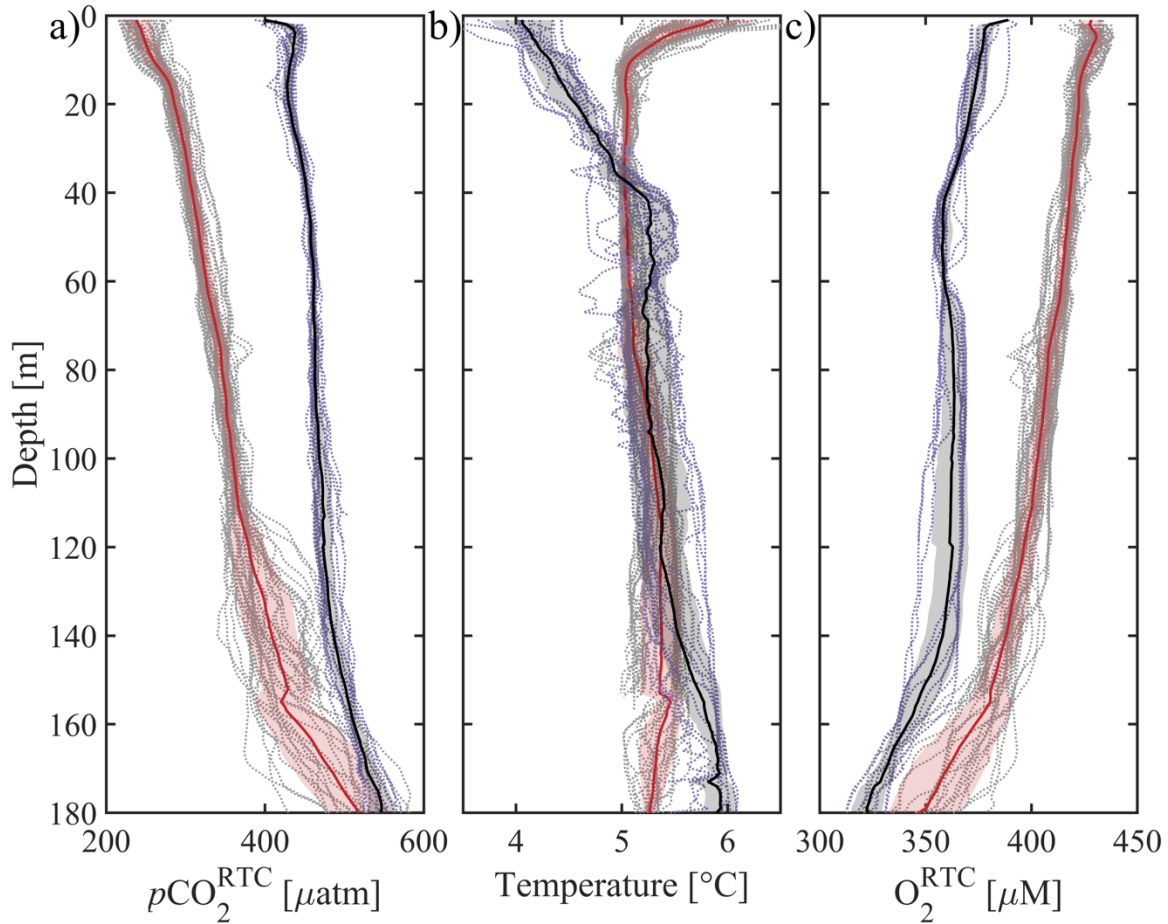
Figure 10. Averaged CO₂ Seaglider profiles from May 2022 and February 2023 missions in Resurrection Bay, Seward, Alaska. Depth profiles of all 1-meter binned dives (dotted gray), average 1-meter binned dive from May 2022 mission (red thick line, dive#1-51, May 5, 2022 00:01 to May, 7 2022 16:37) and February 2023 mission (black thick line, dive#1-17, February 8, 2023 20:50 to February 9, 2023 19:54) with shading showing the standard deviation of the values in each bin added and subtracted from the average. a) Response time corrected pCO_2 ($pCO_2{}^{RTC}$, μatm), b) temperature [°C], and c) response time corrected oxygen ($O_2{}^{RTC}$, μM).

1080
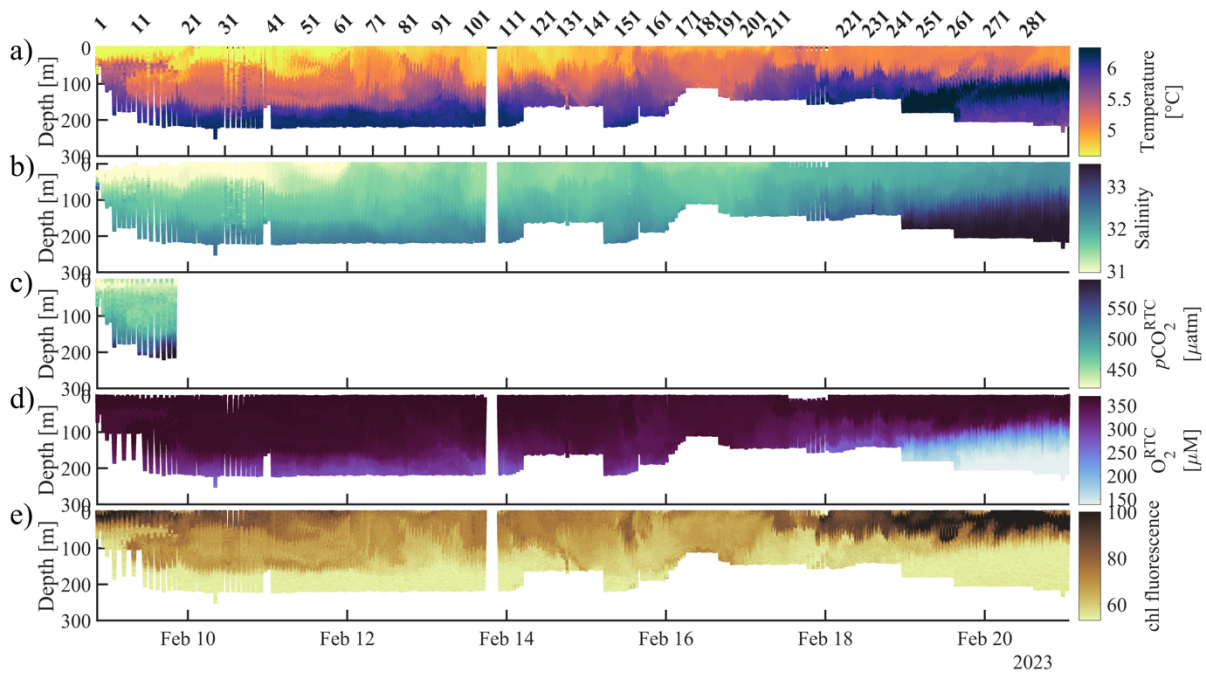
1081

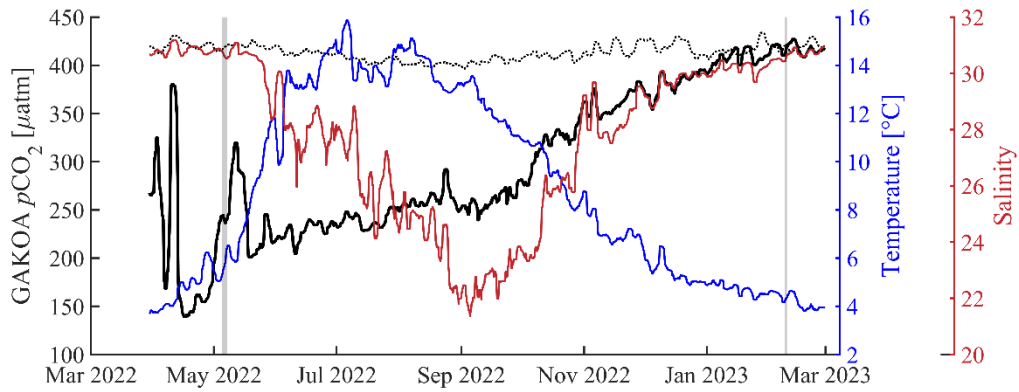1082 **Figure 11. CO₂ Seaglider data collected during the winter mission (February 8 - 21, 2023).**

1083 Shown are a) temperature (°C), b) salinity, c) response time corrected pCO_2 (pCO_2^{RTC}, µatm), d)

1084 response time corrected oxygen (O_2^{RTC}, µM), and e) raw chlorophyll fluorescence (chl

1085 fluorescence) as time/dive number vs. pressure.

1086

1087

1088

Figure 12. National Oceanic Atmospheric Administration's Gulf of Alaska ocean acidification surface time-series from March 2022 - 2023. Left axis sea surface (dotted black line) and air (black line, 4 meter above sea level) pCO_2 [uatm] and right axes sea surface temperature (blue, °C) and sea surface salinity (red). All data shown as 3 day running mean. Vertical shaded gray areas highlight the CO_2 Seaglider missions in May 2022 and February 2023. The mooring is located at 59.911 °N, -149.35 °W (Monacci et al., 2023).

1089

1090

1091

1092

1093

1094

1095

1096

1097

1098